SEMI-ANNUAL REPORT:

RESPONSE OF JOINT DOMINATED SPACE STRUCTURES

CARNEGIE INSTITUTE OF TECHNOLOGY

CARNEGIE MELLON UNIVERSITY

MAY, 1987

1. INTRODUCTORY COMMENTS

This document reports the work completed on the NASA research grant NAG-1-612, entitled, "Response of Joint-Dominated Space Structures". The work falls into two categories: 1) developing an efficient method for calculating the transient response of a non-linear system such as a large joint-dominated space structure and 2) investigating the effect of gravitational loading and joint scaling on the dynamic response of model structures. The progress to date on these two topics is reported in Section 2 and Section 3, respectively.

The research on developing an efficient method for computing transient response is complete and no further technical work will be performed on that topic as part of this contract, although Section 2 is a preliminary draft and will be revised for the final report. Additional work is in progress on joint scaling and will be completed by the end of the contract period.

2 Transient Response of Joint Dominated Space Structures: A New Linearization Technique

by

Gerhard Andrew Foelsche

Report SM-87-3 May 1987

Submitted in partial fulfillment of the
requirements for the degree of
Master of Engineering at Carnegie-Mellon University

Department of Mechanical Engineering
Carnegie Institute of Technology
Carnegie-Mellon University
Pittsburgh, Pennsylvania

Table of Contents

Transient Response of Joint Dominated Space Structures: A New Linearization Technique

by

G. A. Foelsche, J. H. Griffin, J. Bielak

Abstract

A new and efficient linearization method is presented for use in calculating the transient response of non-linear systems. The method is an extension of the describing function approach in which the steady state response of the system is calculated by representing the nonlinear element, typically joints in the the case of space structures, by impedances which are functions of the amplitude of response. As a result, the problem of solving the differential equation for the steady state response becomes one of solving a set of nonlinear algebraic equations involving the steady state amplitudes and phases of the system. For the transient case the steady state impedances can be averaged over the range of response in order to provide equivalent values of stiffness and damping that, for a given set of initial displacements, may be treated as being constant for purposes of calculating system response.

Single-degree-of-freedom systems are used first to demonstrate the method and then to develop an approach for optimizing the joint's characteristics so as to minimize transient response times. The use of this method for response estimation and optimization in multiple-degree-of-freedom systems is investigated subsequently.

Introduction

An important problem in the design of space structures is how to predict their dynamic response. This process is particularly difficult when dealing with structures that contain a large number of joints that exhibit nonlinear, hysteretic behavior. For example, this may be the case for prefabricated truss structures that are designed to collapse into a dense package for transportation to orbit. The truss is then expanded in space by utilizing joints that are specially designed to rotate and lock into place. The dynamic response of such structures is said to be joint dominated if the amount of damping or the stiffness of the system is strongly affected by the joints' behavior. If damping in the system is primarily due to joint hysteresis then joint behavior controls the amplitude of the steady state response as well as the rate at which transients decay. Additionally, in some cases, joint flexibility can significantly reduce the stiffness of the structure, thus reducing its natural frequencies and altering the associated mode shapes. This paper discusses a new approach that may be used to efficiently estimate the transient response of such systems.

The transient response of nonlinear systems is usually calculated by time integration methods that employ finite differences in time. This approach has two disadvantages when it is applied to the design of joint dominated structures. The first is that it is computationally intensive. This would be especially the case for the type of complex three dimensional truss structures that are proposed for space applications since they have a large number degrees of freedom. Secondly, the problem is nonlinear and, consequently, the solutions lack generality. For example, the rate of decay of a transient would depend on the specific magnitude and distribution of the assumed initial displacements and velocities.

Since the number of degrees of freedom is large, it is not reasonable to consider all possible initial conditions. So one difficulty that faces the design engineer is trying to select those conditions that are of critical importance to the design and to simulate the corresponding system response. Neither the selection nor the simulation process is particularly feasible if time integration is the only procedure available for calculating the response of the system.

In this paper an approximate method is developed for estimating the transient response of nonlinear systems in terms of linearized modes of response. Its advantages are that it is computationally more efficient than the time integration method and that it is possible to view the design problem in the more traditional physical terms of modal response. For example, if it is most important to damp the larger amplitude, low frequency response one can easily focus on that issue by isolating the response of the first few linearized modes. Consequently, by utilizing this approach the design problem should become more tractable. The major drawback of the approximate method is loss of accuracy. It is our view that both approximate methods and time integration have their roles in design. Approximate methods provide efficient tools for performing parametric studies and they supply physical insights into how to optimize system performance that are not easily inferred from strictly numerical methods. Time integration provides a method for assessing the accuracy of the approximate solution for key simulations and for fine tuning the final design.

In the procedure presented here the nonlinear system is approximated by an equivalent linear system in which the system parameters are constant over the range of transient response. The method is an extension of the describing function approach used to calculate the steady state harmonic response of nonlinear systems. In the describing

function approach the response is assumed to be essentially harmonic and the nonlinear element is represented by impedances which depend on the amplitude of response. As a result, the problem of solving the differential equation for the steady state response becomes one of solving a set of nonlinear algebraic equations for the steady state amplitudes and phases associated with the various degrees of freedom of the system. In the transient case considered here the steady state impedances are averaged over the range of response in order to provide equivalent values of stiffness and damping that, for a given set of initial conditions, may be treated as constants for purposes of calculating system response. We refer to this approach as the Amplitude Averaging (AA) Method. Once equivalent parameters are identified for the system, conventional methods can be employed for analyzing the resulting linear system.

The AA Method is derived from an efficient time integration procedure presented by Sinha and Griffin [2] in which single time steps were used to step from one peak of the oscillation to the next. Their approach in turn, was based on an idea originally developed by Caughey [1] that the response may be approximated as a sinusoid in which the amplitude and phase vary slowly with time.

In the first part of this paper the AA Method is illustrated by applying it to a single-degree-of-freedom (SDF) system exhibiting the bilinear hysteretic behavior typically associated with Coulomb friction. While the method is not restricted to this type of nonlinearity this behavior was selected for analysis because it is representative of the type of nonlinearity that occurs in actual joints. A half cycle method similar to that used by Sinha and Griffin is presented in order to illustrate the linearization process and in order to develop "instantaneous" values of the nonlinear element's stiffness and damping. The instantaneous values of the element's parameters, which effectively characterize the joint's

properties at a given amplitude of response, are then averaged over a range of amplitudes in order to calculate the constant stiffness and damping values used in the AA Method. Since an equivalent, constant damping has been determined for the system it may be used to select joint characteristics (the friction slip load in this example) so as to maximize average joint damping and minimize transient response times. In the second part of the paper a general approach that may be used for multiple-degree-of-freedom (MDF) systems is given and applied to the two body problem. In each case, the accuracy of the approach is assessed by comparing results from the approximate method with those obtained using standard time integration methods.

Single Degree of Freedom Systems

In order to demonstrate the AA Method, we develop a solution for the SDF system depicted in Fig 1. This is essentially the same system whose steady state behavior was investigated by Griffin *et. al.* in [2], [3], and [4].

The equation of motion for the system is

$$m\ddot{x} + c\dot{x} + kx = -f_n \qquad (1)$$

where f_n is the nonlinear force from the friction element and superscript dots represent differentiation with respect to time. During oscillation, the friction joint remains locked until the magnitude of the spring force $|k_d(x-y)|$, equals the friction force μN . The joint then slips with a constant resistive force of magnitude μN until the mass reaches an extremum of oscillation, at which point the joint locks up again. The relative displacement $(x-y)$ required to cause slip is designated as x_{crit} , where

$$x_{crit} = \frac{\mu N}{k_d} \qquad (2)$$

The Half-Cycle Method

If the transient response is approximately a sinusiod that has an amplitude and phase which vary slowly with time, then over a limited time span it may be approximated as $x = B \cos \theta$, where $\theta = \omega t - \phi$. We assume that the nonlinear force f_n exhibits the same periodicity. Expressing f_n in a Fourier series, we obtain (see Menq and Griffin, [3])

$$f_n = F_c(B) \cos \theta + F_s(B) \sin \theta + \ldots \text{(higher harmonics)} \qquad (3)$$

where

$$F_c(B) = \frac{k_d B}{\pi} \left[\theta^*(B) - \frac{1}{2} \sin 2\theta^*(B) \right] \tag{4}$$

$$F_s(B) = -\frac{4\mu N}{\pi} \left(1 - \frac{\mu N}{k_d B} \right) \tag{5}$$

$$\theta^*(B) = \cos^{-1} \left(1 - \frac{2\mu N}{k_d B} \right) \qquad 0 \leq \theta^* \leq \pi \tag{6}$$

In the case of Coulomb friction, F_c and F_s may be calculated analytically as indicated. In the case of experimental joint data, the Fourier coefficients can be calculated numerically from hysteresis curves.

If we keep only the fundamental harmonics and truncate the expression (3) after the first terms, we can express f_n as

$$f_n = \frac{F_c(B)}{B} x + \frac{-F_s(B)}{\omega B} \dot{x} \tag{7}$$

Thus (1) becomes,

$$m \ddot{x} + \left(c - \frac{F_s}{\omega B} \right) \dot{x} + \left(k + \frac{F_c}{B} \right) x = 0 \tag{8}$$

or,

$$m \ddot{x} + c_{eff}(B) \dot{x} + k_{eff}(B) x = 0 \tag{9}$$

where c_{eff} and k_{eff} are defined in a manner consistent with (8) and are referred to as the instantaneous damping and stiffness of the bilinear spring. In a more familiar form we may write (9) as

$$\ddot{x} + 2\zeta\omega_n \dot{x} + \omega_n^2 x = 0 \tag{10}$$

where ζ and ω_n are both functions of B

$$\zeta(B) = \frac{c_{eff}(B)}{2\sqrt{m\, k_{eff}(B)}} \tag{11}$$

$$\omega_n(B) = \sqrt{\frac{k_{eff}(B)}{m}} \tag{12}$$

The damped natural frequency of this system may be similarly defined as

$$\omega_d(B) = \sqrt{\frac{(1 - \zeta^2(B))\, k_{eff}(B)}{m}} \tag{13}$$

It is observed that during transient oscillation of the nonlinear system , the response is similar to the decaying sinusiod seen in linear analysis. It is reasonable to assume that the motion of the nonlinear system from one extremum of oscillation to the next extremum is representable as the decay of a linear system over a half-cycle. As an example, we consider a system decaying from initial conditions of some initial displacement B_0 and zero initial velocity. Let B_i denote the amplitude of the i^{th} extremum (occuring at time t_i) and B_{i+1} denote the amplitude of the next extremum (at time t_{i+1}) . Then from linear theory, the time elapsed between one extremum and the next is approximately

$$\Delta t = t_{i+1} - t_i = \frac{\pi}{\omega_d(B_i)} \tag{14}$$

and the relationship between successive peaks is

$$B_{i+1} = -B_i\, e^{-\left(\frac{\zeta_i \pi}{\sqrt{1-\zeta_i^2}}\right)} \tag{15}$$

Given the initial amplitude B_o , we can efficiently estimate successive extrema and the time increments at which they occur from (14) and (15). Since the extrema occur each half cycle, we refer to this method as the Half-Cycle Method.

This Half-Cycle Method is an efficient way of approximating a

numerical time integration to find extrema of transient oscillation. Tests on SDF systems show that this method is accurate for nonlinear systems in which $\varepsilon = k_d / (k + k_d) < 0.5$ and provides a reasonable approximation for the amplitude of response for $\varepsilon > 0.5$. The Half-Cycle Method results were compared to more accurate solutions generated by 4^{th} order Runge-Kutta time integration. The comparison of the half cycle estimates to the more exact numerically generated solutions is shown in Figures 2a-d, where the Half-Cycle estimates of the extrema of response are shown as points (the exponential decay envelopes pictured are a result of the new Amplitude Averaging Method and will be discussed later). For nonlinearities $\varepsilon > 0.5$, the system experiences a biasing which is not accounted for in the Half-Cycle Method . However, the peak-to-peak amplitude estimates are seen to be reasonable despite this offset. Note that $\varepsilon > 0.5$ corresponds to severe nonlinearities that are probably much stronger than those that could occur in space stuctures. It may be observed that this approach usually yields conservative estimates of system behavior in that it overestimates the amplitudes of response.

Amplitude Averaging Method

We now introduce a new linearization called the Amplitude Averaging (AA) Method. In this approach, the half-cycle values of damping and stiffness are averaged over the entire response range of interest. Consequently, while these average values are nonlinear functions of the initial displacement, they are constants as far as the transient response analysis is concerned.

The AA Method is also based on equations (3) through (6). Linear, constant parameters are derived by averaging c_{eff} and k_{eff} from (9) over the nonlinear range of oscillation, *i.e.*

$$\overline{c_{eff}}(B_o) = c + \overline{c_e}(B_o) = c + \frac{\int_{x_{crit}}^{B_o} \frac{-F_s(B)}{B\,\omega}\, dB}{B_o - x_{crit}} \qquad (16)$$

$$\overline{k_{eff}}(B_o) = k + \overline{k_e}(B_o) = k + \frac{\int_{x_{crit}}^{B_o} \frac{F_c(B)}{B}\, dB}{B_o - x_{crit}} \qquad (17)$$

where ω in (16) is given by (12). After averaging, (8) becomes

$$m\ddot{x} + (c + \overline{c_e}(B_o))\dot{x} + (k + \overline{k_e}(B_o))x = 0 \qquad (18)$$

For the example of Coulomb friction, the analysis can be simplified by expressing the averaged properties in terms of several nondimensional parameters: (nondimensionality indicated by a * superscript)

$$\overline{k_e}(B_o) = k_d\, \overline{k_e^*}(B_o^*) \qquad (19)$$

$$\overline{c_e}(B_o) = \frac{c_o}{\overline{\omega^*}(B_o^*)}\, \overline{c_e^*}(B_o^*) \qquad (20)$$

where

$$c_o = 2m\omega_o = 2\sqrt{m k_d} \qquad (21)$$

$$\overline{\omega^*}(B_o^*) = \sqrt{\frac{k}{k_d} + \overline{k_e^*}(B_o^*)} \qquad (22)$$

and

$$B_o^* = \frac{B_o}{x_{crit}} = \frac{B_o k_d}{\mu N} \qquad (23)$$

$\overline{k_e^*}(B_o^*)$ and $\overline{c_e^*}(B_o^*)$ are the nondimensional averaged stiffness and damping of the friction element. These quantities are of particular

interest because their values may be calculated in terms of the single nondimensional parameter, B_o^*, the initial displacement.

For Coulomb friction from (4), (17), and (19), $\overline{k_e^*}$ is given by

$$\overline{k_e^*}(B_o^*) = \frac{1}{\pi\,(B_o^* - 1)} \int_1^{B_o^*} \{\, \theta(B^*) - 0.5 \sin[\,2\,\theta(B^*)\,]\,\}\, dB^* \qquad (24)$$

where

$$\cos\theta(B^*) = 1 - \frac{2}{B^*} \qquad , \quad (B^* \geq 1)$$

and need be calculated only once. The nondimensional frequency $\overline{\omega^*}$ is then easily estimated from (12), (17), and (19) as

$$\overline{\omega^*}(B_o^*) = \sqrt{\frac{k}{k_d} + \overline{k_e^*}(B_o^*)} \qquad (25)$$

Lastly, from (5), (16), and (20), the average nondimensional damping is approximated as

$$\overline{c_e^*}(B_o^*) = \frac{2}{\pi\,(B_o^* - 1)} \int_1^{B_o^*} \left\{ \frac{1}{B^*} - \frac{1}{(B^*)^2} \right\} dB^* \qquad (26)$$

which yields upon integration

$$\overline{c_e^*}(B_o^*) = \frac{2}{\pi\,(B_o^* - 1)} \left\{ \frac{1}{B_o^*} + \ln(B_o^*) - 1 \right\} \qquad (27)$$

Note that the parameters are averaged only over the range in which they exhibit nonlinear behavior. The system is linear for amplitudes less than x_{crit} and the response can be calculated using standard methods in that regime.

The AA Method gives a linear estimate of the nonlinear behavior of the system. Results from the AA linearized systems are shown in Figures

2a-d as exponential decay envelopes, and are plotted with the Half Cycle Method and Runge Kutta results for comparison. As with the Half-Cycle Method, we again see conservative estimates of actual system behavior, and again the estimates are more precise for weakly nonlinear systems.

An important result of the AA Method is shown in Figure 3. This figure shows the nondimensional quantities $k_e^*(B_o^*)$, $c_e^*(B_o^*)$, $\overline{k_e^*}(B_o^*)$, and $\overline{c_e^*}(B_o^*)$ in terms of the nondimensional initial displacement B_o^*. It is observed that there are optimal system configurations which maximize either instantaneous or average damping in the system. These optimality conditions depend only on the nondimensional initial displacement B_o^*. Recall from (23) that B_o^* is dependent on the system parameters. Thus, by adjusting just one of these parameters, say, normal load for example, it is possible to optimally damp an existing system. For example, the points A, B, and C on the average damping curve can be thought of as three systems which are identical except for the tightness of the friction joint as indicated by the normal load (normal load = N , $N_A > N_B > N_C$). Comparing the linear average damping terms provided by the AA Method for the three systems, it is seen that system B, with normal load N_B, has the highest value of average damping and is an optimally damped system for this set of basic parameters. The optimality of system B in an average sense was confirmed by 4^{th} order Runge-Kutta simulations. The results for the three systems A, B, and C are shown in Figure 4, where successive extrema have been connected to form an envelope of decay. The normal load N_B is not simply the largest or smallest normal load which could be applied, nor is it the same load which would be required to optimally damp only the first oscillatory swing in the transient motion (this normal load would be present in system D and would be chosen to maximize the position on the instantaneous damping

curve) .

Runge-Kutta simulations confirm the optimality results which were readily provided by the AA Method. We observe, however, that the optimality result would not have been nearly so obvious if an exact time integration had been used alone to investigate this transient behavior. It is also noted that the AA Method provides general results in that it allows for parameter-based comparisons of different systems. Numerical time integration methods lack this generality, yielding instead results which are case-specific and thus more difficult to interpret when comparing systems.

The AA Method leads to systems which are optimized, in an averaged sense, over the entire range of nonlinear behavior. The Half-Cycle Method may be used to generate systems which are optimal in a "first swing" sense. It is also possible to optimize the system over other select ranges of nonlinear behavior. This is done by averaging the c_{eff} and k_{eff} equations over the particular range of concern, resulting in a new curve for $\overline{c_e^*}(B_o^*)$. The optimal normal load (or other parameter) is the one which adjusts the nondimensional initial condition so as to maximize the value of this new $\overline{c_e^*}(B_o^*)$. The linearizations described so far make it possible to optimize the nonlinear system, in an average sense, over any range of nonlinear behavior.

The Amplitude Averaging Method has yielded a general result which was not obvious from numerical time integrations. In the next section, the application of the AA Method to multiple mass systems is developed and it is shown that the principles of generality-of-results and optimal damping still apply, only that they now apply in a modal sense.

Multiple Degree of Freedom Systems

The transient analysis of multiple-degree-of-freedom (MDF) nonlinear systems using the AA Method can be accomplished by representing the system in modal form in terms of a sum of SDF nonlinear systems. The SDF components are linearized separately and are then combined to form a linear representation of the MDF system.

In the linearization process, a nonlinear friction damper will be replaced by linear elements which approximate its behavior, as depicted in Figure 5. This 2DF system incorporates a friction damper as a nonlinear element and will serve to illustrate the application of the Amplitude Averaging Method to MDF nonlinear systems. The equations of motion for the system may be written in matrix form as

$$\mathbf{M}\ddot{\mathbf{x}} + \mathbf{C}\dot{\mathbf{x}} + \mathbf{K}\mathbf{x} = -f_n \begin{bmatrix} 1 \\ -1 \end{bmatrix} \tag{24}$$

where

$$\mathbf{x} = \begin{bmatrix} x_1 \\ x_2 \end{bmatrix}$$

$$\mathbf{M} = \begin{bmatrix} m_1 & 0 \\ 0 & m_2 \end{bmatrix}$$

$$\mathbf{C} = \begin{bmatrix} c_1 & 0 \\ 0 & c_2 \end{bmatrix}$$

$$\mathbf{K} = \begin{bmatrix} k_1 + k_3 & -k_3 \\ -k_3 & k_2 + k_3 \end{bmatrix}$$

MDF Linearization

In the SDF analysis we were able to regard the initial amplitude across the friction damper as the maximum spanning which the joint would experience during transient oscillation. In the MDF system, the initial amplitude across the joint is no longer guaranteed to be the maximum span which the joint experiences. Consequently, the nonlinear system cannot be linearized by simply considering the isolated friction damper and the span across it. This motivates the use of a modal approach in the linearization process.

It is necessary to decouple the nonlinear MDF system of Fig 5 into two SDF nonlinear systems so that the AA Method may be applied to each of the decoupled systems separately. Decoupling of linear systems is done routinely [5],[6] while nonlinear systems are not generally amenable to such analysis. The nonlinear decoupling and modal linearizations may be accomplished with the iterative approach detailed in Appendix I. A set of converged eigenvalues and eigenvectors is obtained and used to form a modal (decoupled) representation of the nonlinear system. The decoupled systems are linearized using the AA Method and are transformed back to the original coordinates to yield a linear MDF system.

Several approximations are made during the decoupling process. Viscous damping is generally small and is, therefore, neglected in order to avoid the inconvenience of dealing with complex eigenvectors. The complex formulation could be pursued in order to increase the overall accuracy of the linearization and estimation scheme. Another assumption made in the analysis is that each modal friction joint operates with the full normal load and coefficient of friction of the physical system. That is, the product μN is unnaffected by the transformation to and from modal coordinates, and may be applied in each mode independently. This

latter assumption is believed to be responsible for the fact that the modal AA response estimates are no longer conservative in some instances.

However, in general the results obtained from the AA Method compare well with results from direct time integration. The modal comparisons for two cases are shown in Figures 6 and 7. where the time integration solutions have been transformed from the original **x** coordinates into the converged modal coordinates, η_1 and η_2 , by using the converged eigenvectors. Overall, the exact modal solution is seen to be similar in form to a decaying sinusiod centered about a zero equilibrium state. The neatness (symmetry and sinusiodal appearance) of the exact modal solution indicates that the converged linear decoupling does in fact represent the nonlinear behavior fairly well, as the response in **x** coordinates would transform poorly if the modal representation was not a reasonable estimate of system response.

In particular, several characteristics of the AA Method as applied to MDF systems are illustrated in Figures 6, 7, and 8. Firstly, the AA estimates in Figures 6 and 7 are no longer conservative. Secondly, while the symmetric sinusiodal form is still obvious in all cases, it is noted that the larger the viscous damping and nonlinearities in a mode, the less "neat" the modal response looks. Thirdly, a MDF system can be modally optimized in a fashion similar to that used to optimize the SDF system. As in the SDF case, the correct manipulation of the normal load shifts the nondimensional modal initial condition to a condition which generates the optimal (modal) damping. It is noted that it is not generally possible to optimally damp both modes simultaneously, as the optimization of one mode results in a detrimental or non-optimizing shift of the other mode. Figure 6 shows a system which is not optimally damped in either mode. Figure 7 shows the same system after the normal load has been adjusted to optimally damp the higher frequency mode (mode 2). The results are

plotted on different scales in Figures 6 and 7 and so it is not immediately obvious that the optimization was successful. However, in Fig 8b , the extrema in the numerical time integration solutions for the non-optimized-mode 2 and optimized-mode 2 systems have been scaled for direct comparison (extrema plotted to form decay envelope). From Fig 8b it is obvious that the optimization has a significant effect on modal response. The same system was optimized in mode 1 in Fig 8a , but in this particular system the friction damping in the first mode was quite small compared to viscous effects, so an expanded scale was used to show the optimization result more clearly. The AA optimization results for both modes 1 and 2 were confirmed by Runge-Kutta simulation. Thus, although the modal AA extrema may be nonconservative in some cases, the AA indication of modal optimality remains accurate.

The AA Method may thus be used to optimally damp select modes of particular concern. This is helpful in the design process in that it gives an easy indication of which systems are optimal in which situations. This knowledge may in turn be used to determine which special physical tests should be run in order to confirm and further refine system models. Again, it may not be possible to control the physical parameters needed to accomplish this modeled optimality, in which case the issue may become one of selecting the most nearly optimal configuration from a variety of available designs.

Conclusion

This paper has discussed the specific application of the Amplitude Averaging Method to friction damped systems. However, the AA Method is a more general linearization method applicable not only to friction damped systems but also to other systems which exhibit nonlinear hysteretic behavior.

The AA Method is efficient and can be used to easily establish optimization conditions, subject to time integration verification. Familiar modal analysis may be applied to MDF nonlinear systems and systems may be optimized over specific ranges of nonlinear oscillation. Furthermore, the AA Method can be used to modally optimize MDF systems in order to suppress system response over specific frequency ranges.

The AA Method may also be used as a comparison tool in the system design process. The physical parameters of the system may not be adjustable to the indicated optimal values. For example, in the case of jointed structures and friction damping, it is not generally possible to select physical joints with adjustable (optimizable) normal loads. In this situation the task may be one of selecting joints from a variety of designs. The AA Method yields the relative averaged damping in these designs for amplitudes of response which are representative of those encountered in practice and thus may be employed as a method of comparison in order to help choose the most nearly optimal design.

The AA Method is an efficient design tool for two reasons. The first reason is that the method is computationally efficient. In the cases considered in this paper, AA solutions could be calculated an order of magnitude more quickly than numerical time integration solutions. In addition, the method is efficient because it provides a sytem representation in terms of linearized modes and, consequently, it becomes

relatively easy to establish optimum system response. Again, it is our view that numerical time integration and the AA Method are complimentary approaches and that both have their places in the design and analysis of nonlinear systems. The AA Method is a computationally un-intensive approach which supplies analytical insight at the expense of accuracy, while the time integration approach provides verification and fine tuning of the results for select cases of interest.

Bibliography:

1 Caughey, T. K., "Sinusiodal Excitation of a System With Bilinear Hysteresis," *ASME Journal of Applied Mechanics*, Vol. 27, 1960, pp. 640-643

2 Sinha, A., and Griffin, J. H.,"Effects of Static Friction on the Forced Response of Frictionally Damped Turbine Blades," *ASME Journal of Engineering for Gas Turbines and Power*, Vol. 106, Jan. 1984, pp. 65-69

3 Menq, C.-H., and Griffin, J., H., "A Comparison of Transient and Steady State Finite Element Analyses of the Forced Response of a Frictionally Damped Beam," *ASME Journal of Vibration, Acoustics, Stress, and Reliability in Design*, Vol. 107, Jan. 1985, pp. 204-210

4 Griffin, J. H., "Friction Damping of Resonant Stresses in Gas Turbine Airfoils," *ASME Journal of Engineering for Power*, Vol. 102, Apr. 1980, pp. 329-333

5 Thomson, William T., *Theory of Vibrations With Applications*, Second Ed., Prentice-Hall, New Jersey, 1981, pp 132-201

6 Craig, Roy R. Jr., *Structural Dynamics: An Introducyion to Computer Methods*, Wiley and Sons, New York, 1981, pp 273-375

7 Den Hartog, J. P., "Forced Vibrations With Combined Coulomb and Viscous Friction," *Transactions of ASME*, 1931, pp. 107-115

8 Menq, C.-H., Griffin, J., H., and Bielak, J., "The Influence of Microslip on Vibratory Response; Part 1: A New Theoretical Model", *Journal of Sound and Vibration*, Vol.107, pp. 279-293

9 Menq, C.-H., Griffin, J., H., and Bielak, J., "The Influence of Microslip on Vibratory Response; Part 2: A Comparison to Theoretical Results", *Journal of Sound and Vibration*, Vol. 107, pp. 295-305

A. ITERATIVE METHOD FOR DECOUPLING AND LINEARIZING A NONLINEAR MDF SYSTEM

This method neglects damping in determining the eigenvectors of the system. This is a reasonable approximation for slightly damped systems. There are seven steps in the process. They are illustrated by applying them to the two degree of freedom (2DF) system of Figure 5

1. Write the governing equation of the system in matrix form, neglecting viscous damping, e.g., for the 2DF system of Figure 5

$$M_o\ddot{x} + K_o x = f_n \begin{bmatrix} -1 \\ 1 \end{bmatrix} \tag{A.1}$$

2. Find the eigenvalues and eigenvectors of the linear part of the system, momentarily disregarding the nonlinear term f_n. Form the matrix of eigenvectors, Φ, e.g.,

$$K_o\phi_i = \lambda_i M_o \phi_i \qquad \text{eigenvalues } \lambda_1, \lambda_2$$

$$\text{eigenvectors } \phi_1 = \begin{bmatrix} \phi_{11} \\ \phi_{21} \end{bmatrix} \qquad \phi_2 = \begin{bmatrix} \phi_{12} \\ \phi_{22} \end{bmatrix} \tag{A.2}$$

$\Phi = [\phi_1, \phi_2]$ ... matrix of eigenvectors.

3. Assume x can be represented in terms of modal coordinates η

$$x = \Phi\eta \tag{A.3}$$

then

$$\eta = \phi^{-1}x$$

The modal initial conditions can be found using (A.3) and the orthogonality of the eigenvectors (with respect to M)

$$\eta_o = \Phi^{-1}x_o$$

4. Form a decoupled set of equations by substituting $x = \Phi\eta$. Step 3 into the governing equation from Step 1

$$M_o\Phi\ddot{\eta} + K_o\Phi\eta = f_n \begin{bmatrix} -1 \\ 1 \end{bmatrix}$$

$$\Phi^T M_o \Phi \ddot{\eta} + \Phi^T K_o \Phi \eta = \Phi^T f_n \qquad \begin{bmatrix} -1 \\ \\ 1 \end{bmatrix}$$

5. Find linearized stiffnesses for each independent mode using the AA method. This step yields

$$\Phi^T M_o \Phi \ddot{\eta} + \Phi^T K_o \Phi \eta = - K_q \eta - C_q \dot{\eta}$$

(Analogous to:

$$- f_n = - \frac{F_c}{B} x + \frac{F_s}{\omega B} \dot{x} \Rightarrow - k_e x - c_e \dot{x}$$

as done in the SDF case in equations (7,8,16,17,18) in the main body of the paper.) K_q is a diagonal matrix, each diagonal element is the linearized stiffness of the friction element in its respective mode, e.g., in the example 2DF system, slip occurs when

$$\mu N = k_d (x_1 - x_2)$$

or

$$\mu N = k_d [1 \; - 1] x$$

substitute equation from Step 3

$$\mu N = k_d [1 \; - 1] \Phi \eta \qquad \Phi = [\phi_1 \; \phi_2] = \begin{bmatrix} \phi_{11} & \phi_{12} \\ \phi_{21} & \phi_{22} \end{bmatrix}$$

where $\eta = [\eta_1, \eta_2]^T$. Thus

$$\mu N = k_d [\eta_1 (\phi_{11} - \phi_{21}) + \eta_2 (\phi_{12} - \phi_{22})]$$

Let

$$k_{d_1} = k_d (\phi_{11} - \phi_{21})$$

$$k_{d_2} = k_d (\phi_{12} - \phi_{22})$$

$$\mu N = k_{d_1} \eta_1 + k_{d_2} \eta_2$$

Assume that slip occurs independently in each mode. Then the modal slip conditions are given by

$$\eta_{i_{crit}} = \frac{\mu N}{k_{d_i}} \text{ (analogous to } x_{crit} = \frac{\mu N}{k_d})$$

The modal initial conditions were found in Step 3. Given the initial conditions and the slip conditions, the AA method may be applied to each mode separately in order to linearize the decoupled systems. From the first mode, the linearized stiffness term is $-k_{e_1}$. Mode 2 yields $-k_{e_2}$.

$$\text{Form } K_q\text{: } K_q = \begin{bmatrix} k_{e_1} & 0 \\ 0 & k_{e_2} \end{bmatrix}$$

The linearized modal stiffnesses have been found (C_q is found simultaneously).

6. Convert back to original coordinates:

$$x = \Phi^{-1}\eta$$

Substituting into the linearized governing equation from Step 5:

$$M_o\ddot{x} + K_o x = -\Phi^{T^{-1}} K_q \Phi^{-1} x \quad \text{(neglect } C_q\text{)}$$

define

$$K_{mod} \cong \Phi^{T^{-1}} K_q \Phi^{-1}$$

then

$$M_o\ddot{x} + (K_o + K_{mod})x = 0$$

7. Let $M_1 = M_o$, $K_1 = K_o + K_{mod}$, then

$$M_1\ddot{x} + K_1 x = 0$$

But this system has different eigenvalues and eigenvectors than the original system considered in Step 2. The linearization of Step 5 was heavily dependent on the eigenvectors of the system, which have changed slightly after linearization. To obtain a more accurate linearization, repeat Steps 1-7 using the eigenvectors from the M_1,K_1 system.

The process (Steps 1-7) may be repeated as many times as needed to obtain a converged set of eigenvectors using $M_{(i)}$,$K_{(i)}$. In practice, this method usually converged in 4 iterations and never required more than six iterations to converge.

While the linearized damping is retained and refined in each iteration, it is neglected along with any original viscous damping in the system in order to simplify the

eigenvector and convergence calculations. Consequently, the method is less accurate when high viscous damping or large nonlinearities are present in the system. A complex eigenvalue and eigenvector formulation could be pursued to increase accuracy.

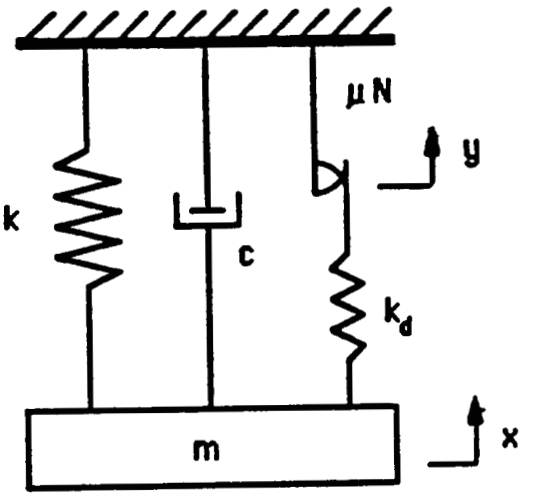

Figure 1a

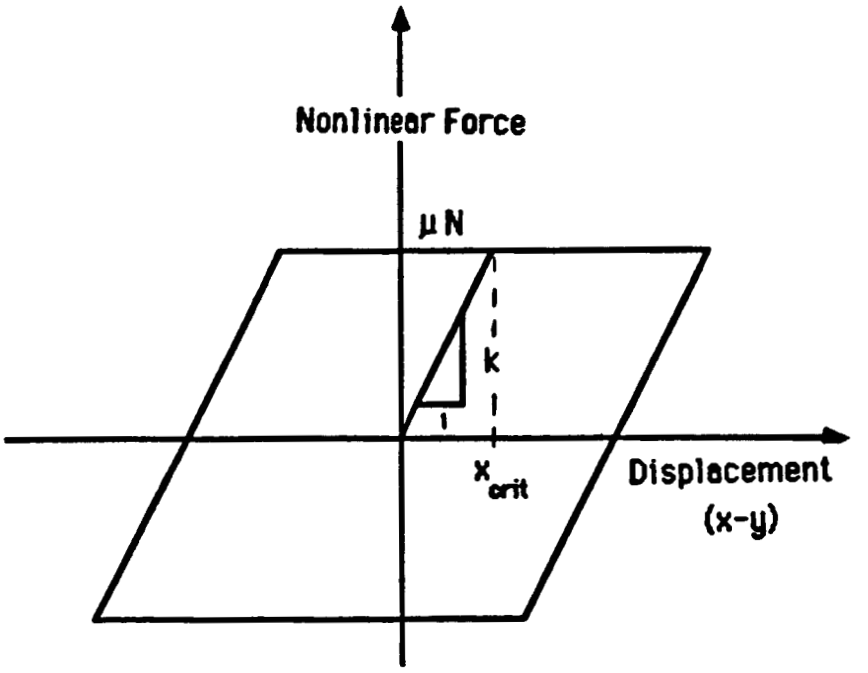

Figure 1b

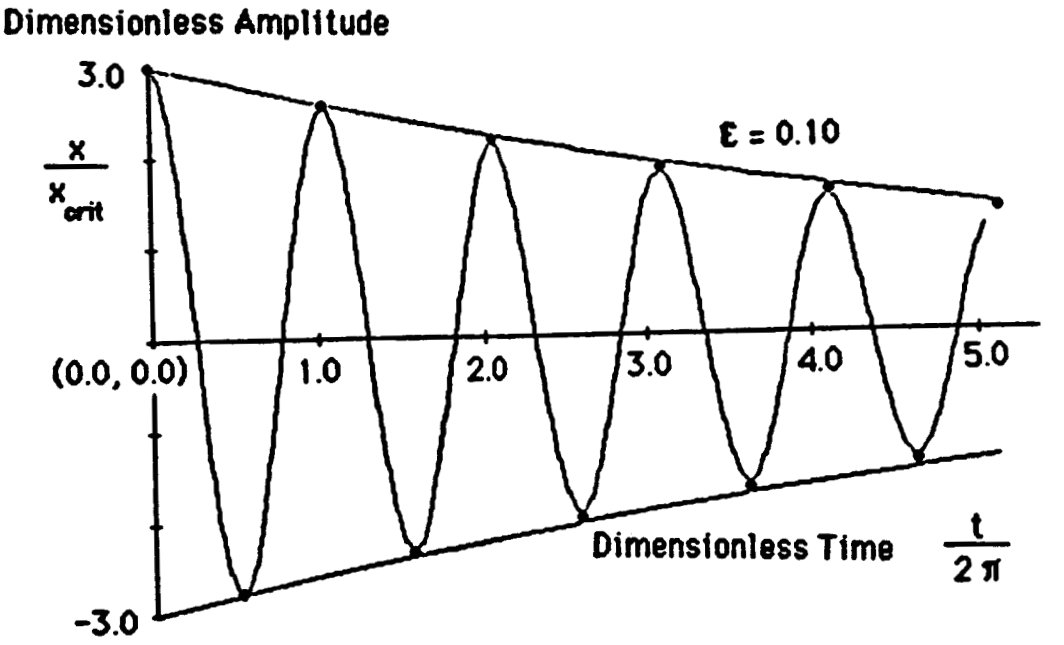

Figure 2a

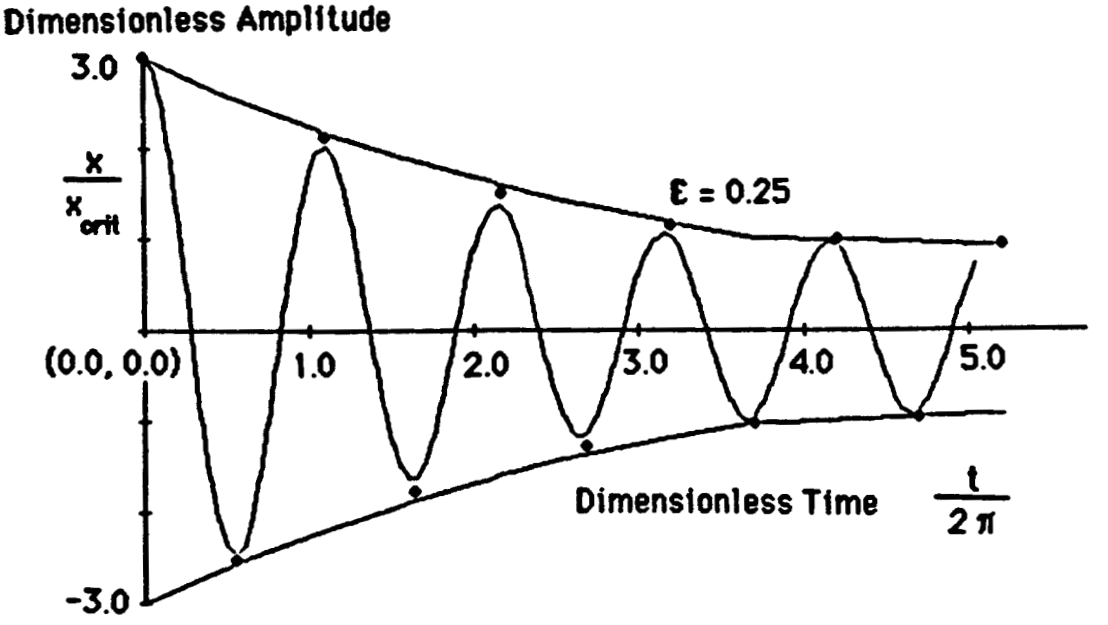

Figure 2b

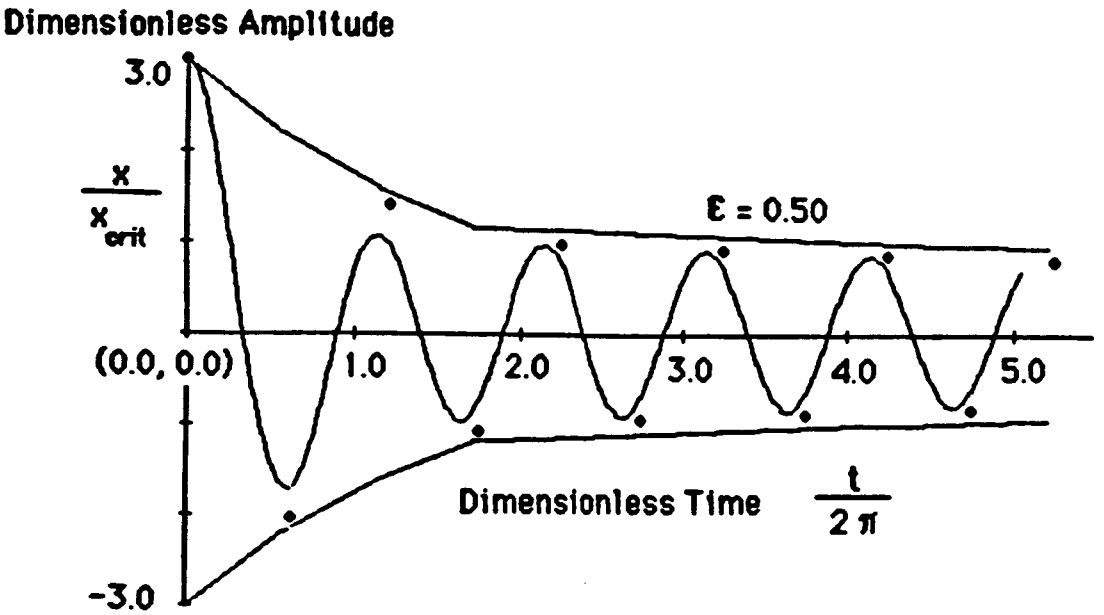

Figure 2c

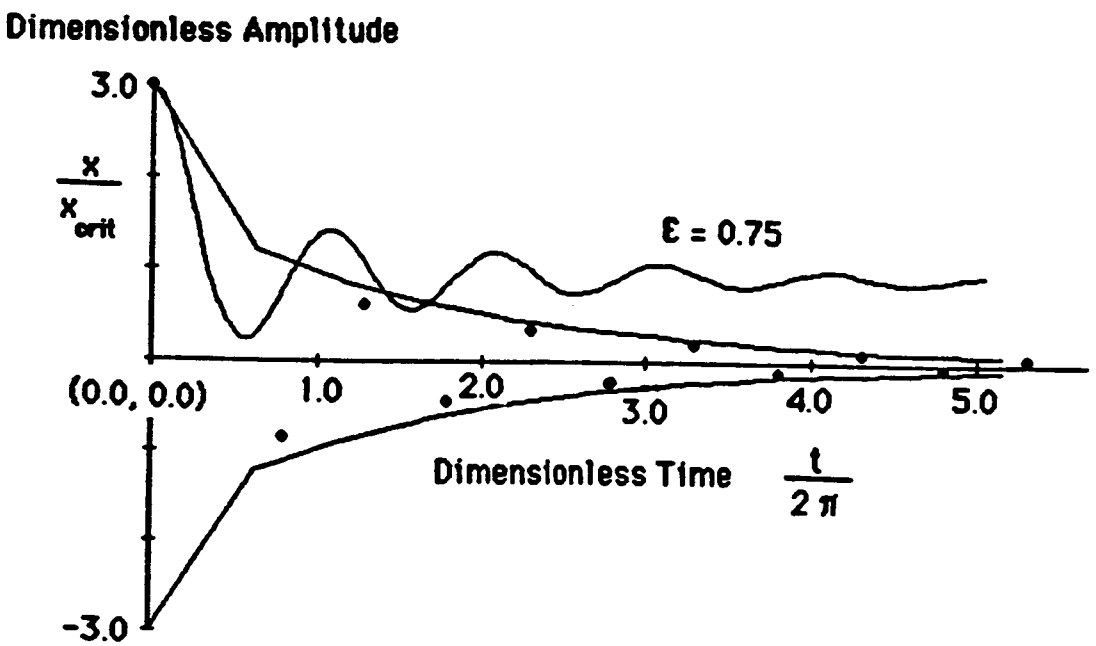

Figure 2d

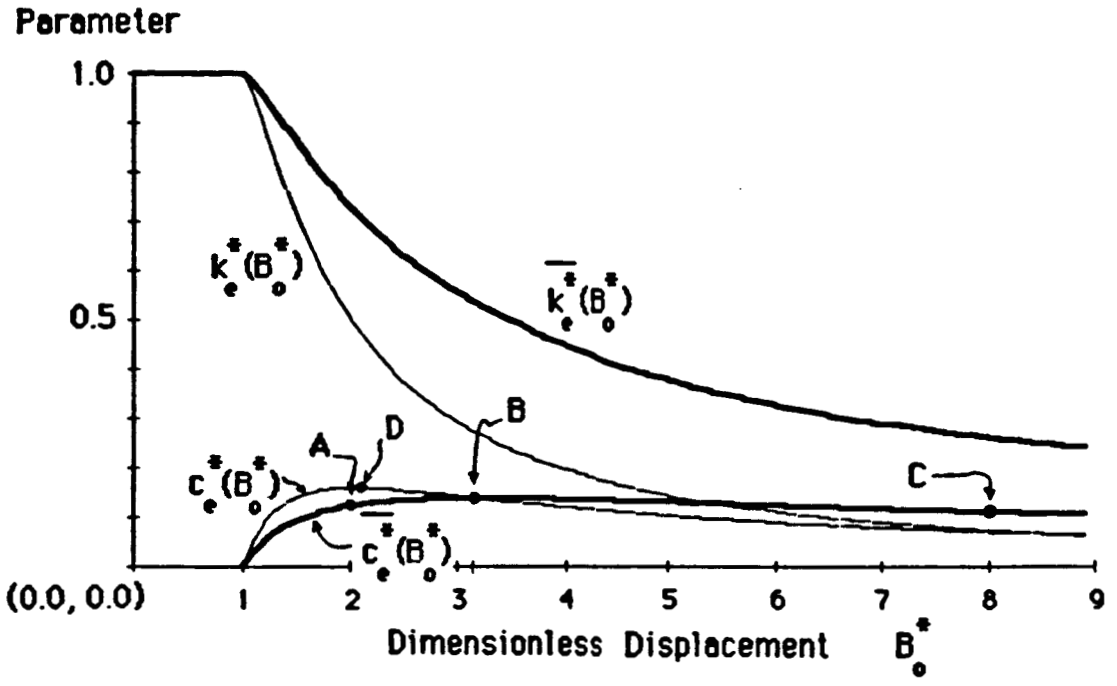

Figure 3

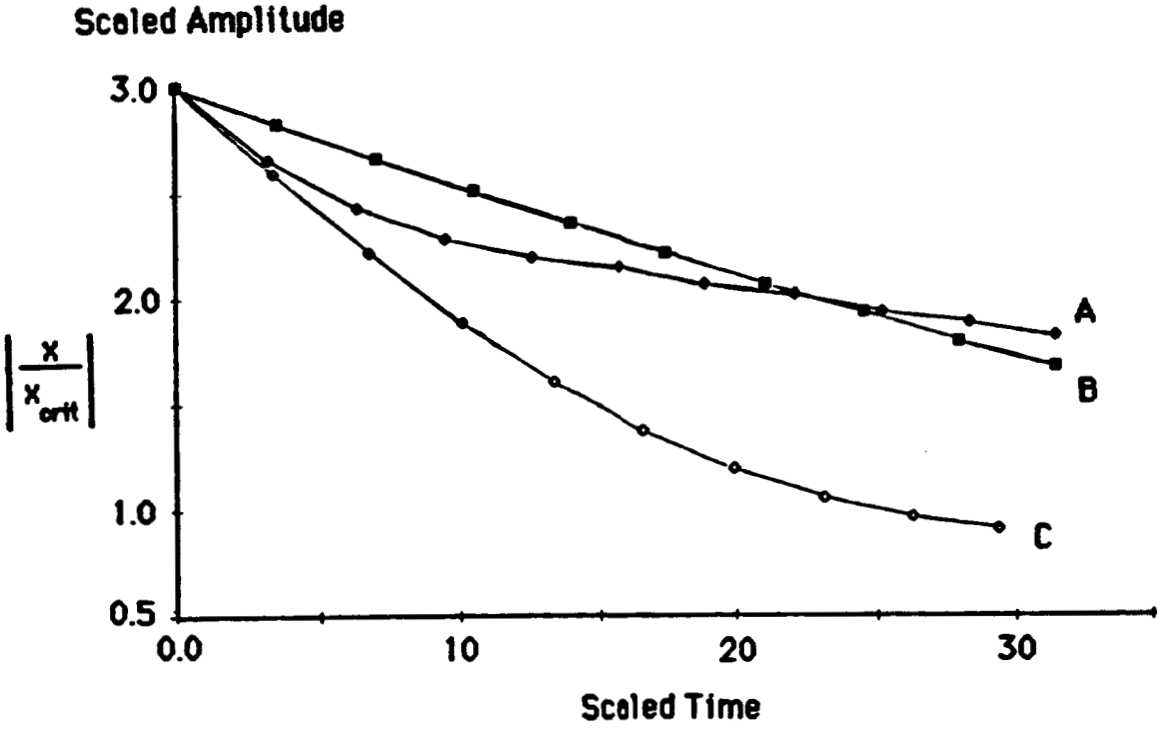

Figure 4

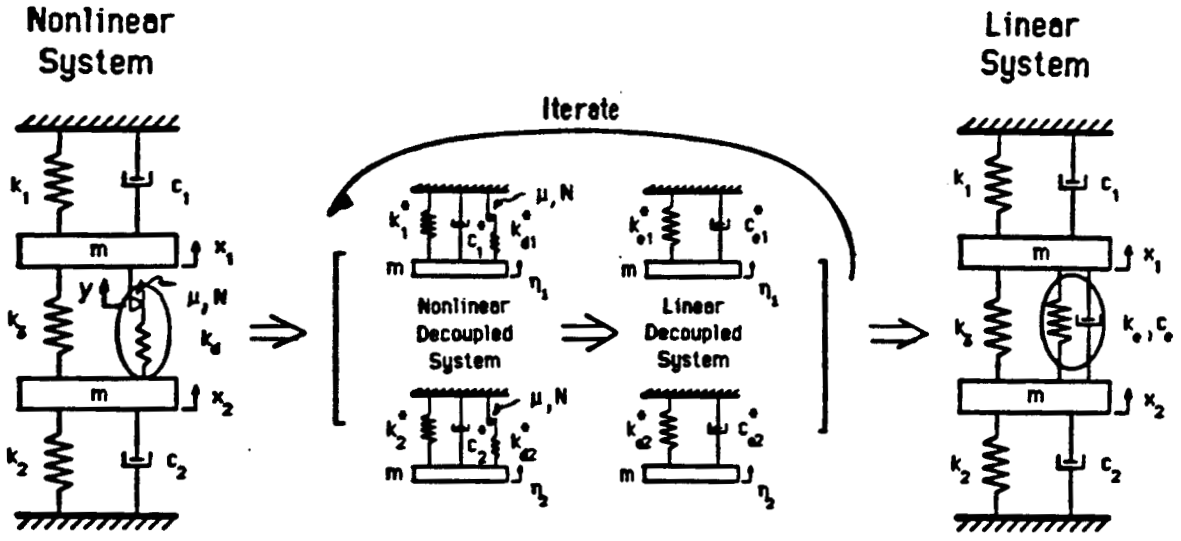
Nonlinear System
Iterate
Linear System
Nonlinear Decoupled System
Linear Decoupled System

Figure 5

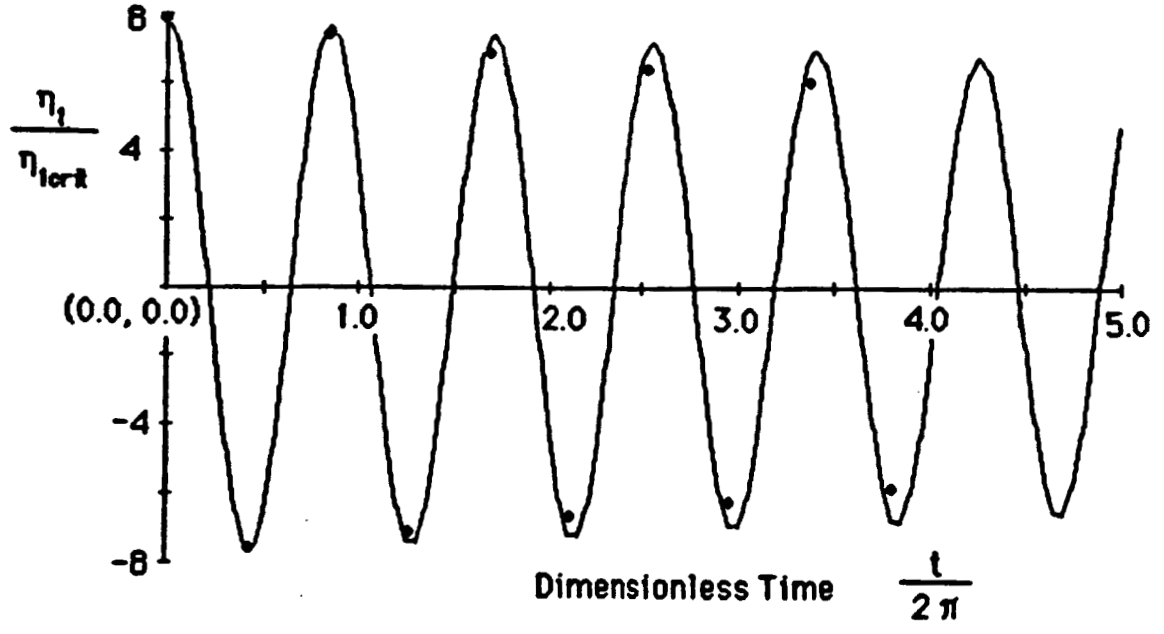

Figure 6a

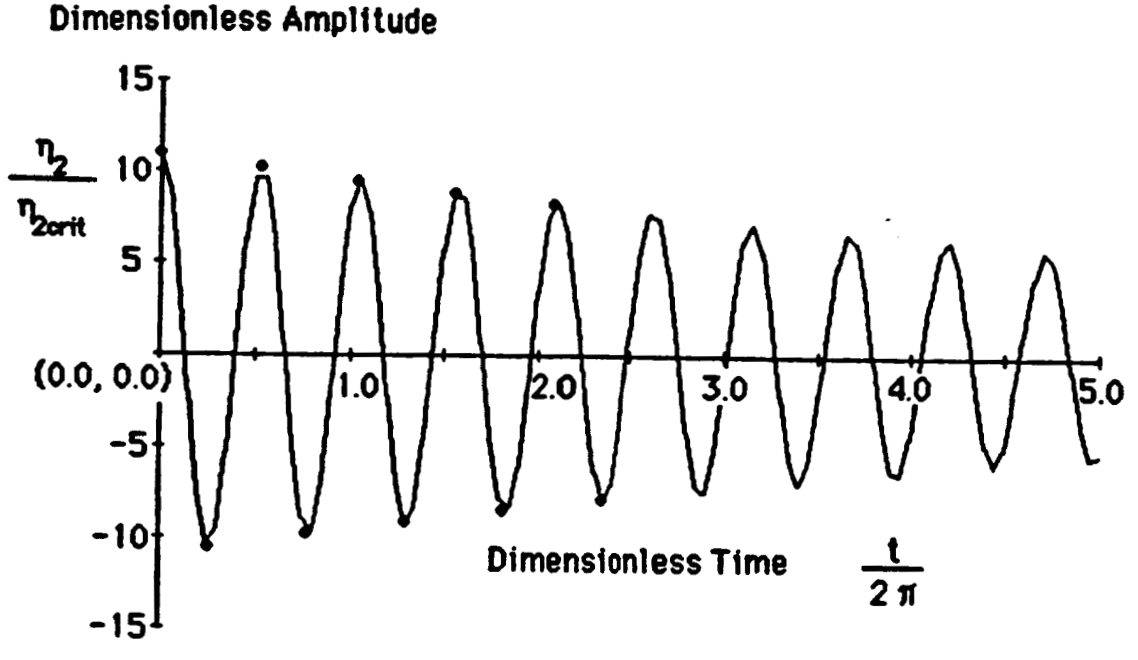

Figure 6b

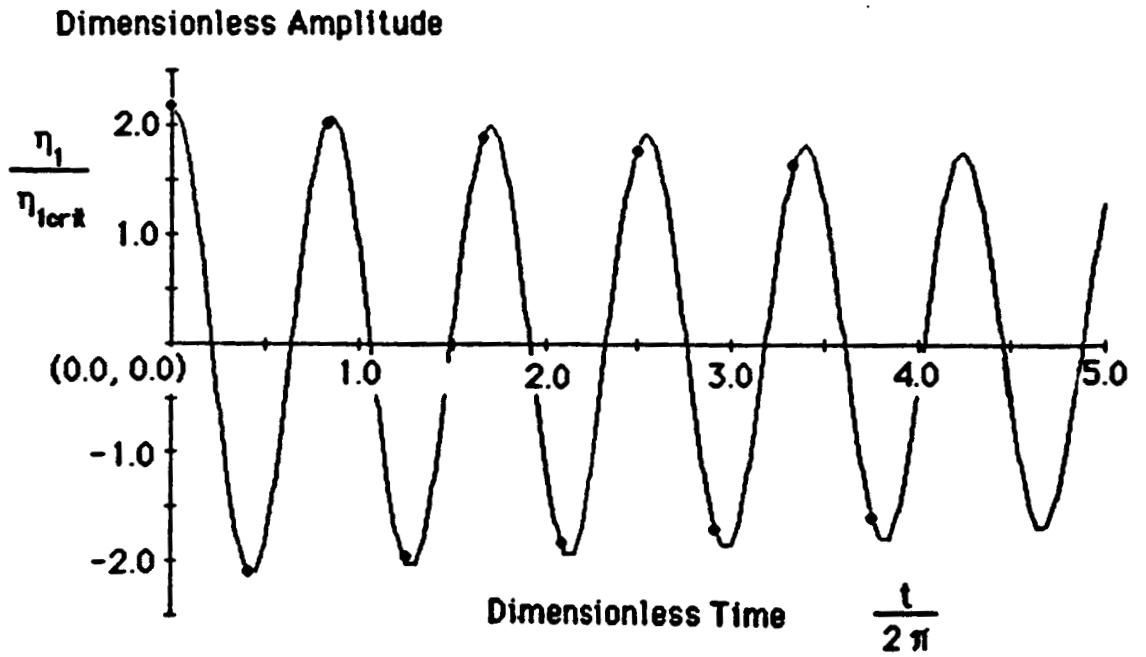

Figure 7a

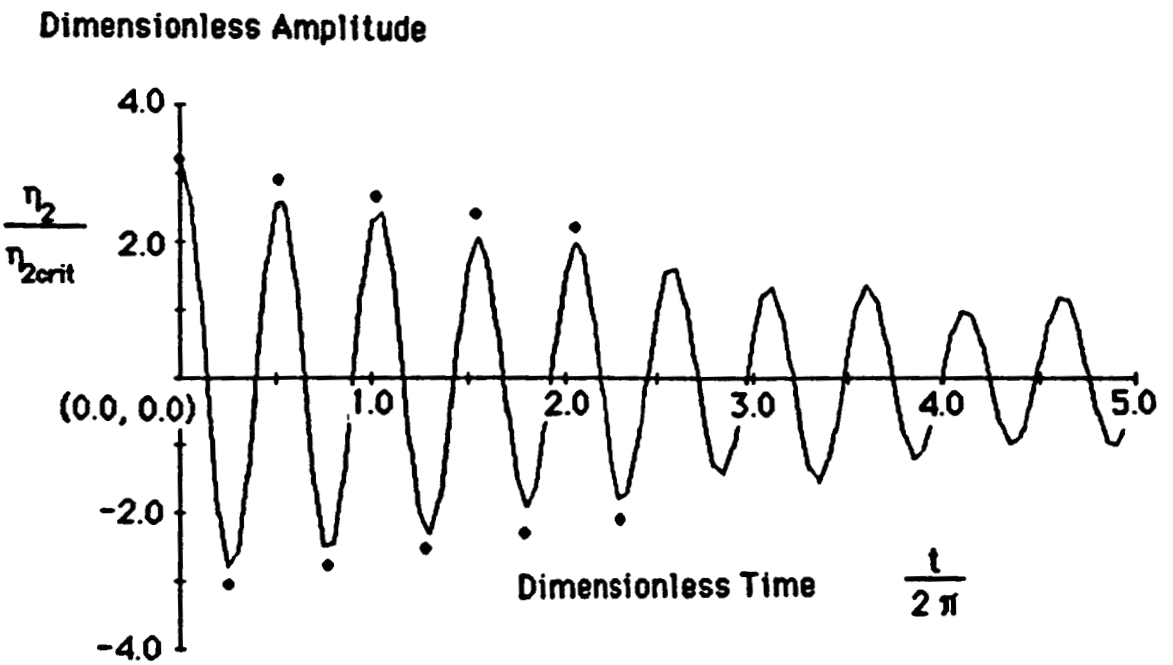

Figure 7b

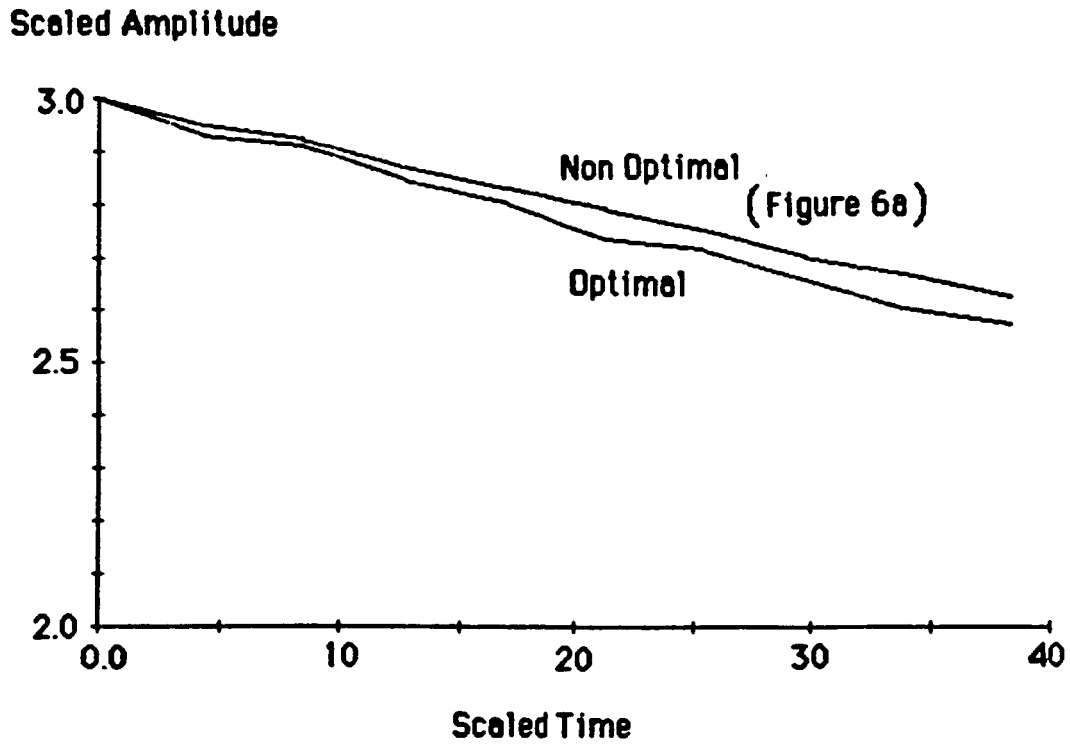

Figure 8a

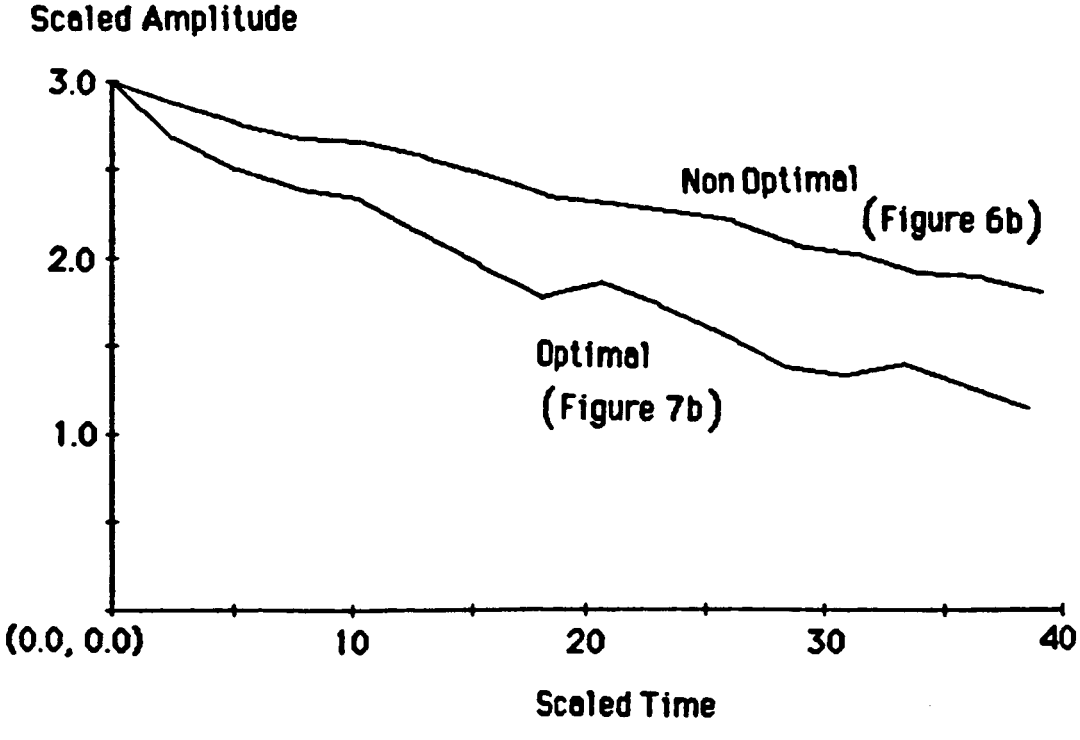

Figure 8b

Figure Captions

Figure 1

a. A single degree of freedom system with Coulomb damper as a nonlinear element.
b. The hysteresis curve for the nonlinear element alone.

Figure 2:

These graphs show system decay from initial displacement conditions x=3.0, y=2.0 and v=dx/dt=0.0. The sinusiodal lines are numerical time integration solutions. The dots are Half-Cycle Method estimates of the response. The exponential decay envelopes were generated by the AA Method. Parameters for each system are given below.

a. m=1, c=0.02, k=0.9, k_d=0.1, μN=0.1
b. m=1, c=0.02, k=0.75, k_d=0.25, μN=0.25
c. m=1, c=0.02, k=0.5, k_d=0.5, μN=0.5
d. m=1, c=0.02, k=0.25, k_d=0.75, μN=0.75

Figure 3:

Instantaneous damping (c_e^*) and stiffness (k_e^*) and average damping ($\overline{c_e^*}$) and average stiffness ($\overline{k_e^*}$). Note maximum of $\overline{c_e^*}$ at $B_o^* \approx 3.16$.

Figure 4:

Comparison of systems A, B, and C from Figure 3. Normal loads (given by N) satisfy $N_A > N_B > N_C$. System B is optimal.

Figure 5:

The linearization used for MDF nonlinear systems.

Figure 6:

System Parameters: $k_1=k_3=m=1.0$, $k_2=2.0$, $c_1=c_2=0.01$, $k_d=0.25$, $\mu N=0.1$, Initial conitions: x1=10.0, x2=2.5, v1=dx1/dt=0.0=v2, (y=9.6, for no immediate slip)

a. Mode #1 response curve
b. Mode #2 response curve

Neither mode is optimal.

Figure Captions

Figure #7:

System Parameters: $k_1=k_3=m=1.0$, $k_2=2.0$, $c_1=c_2=0.01$, $k_d=0.25$, $\mu N=0.35$, Initial conitions: x1=10.0, x2=2.5, v1=dx1/dt=0.0=v2, (y=8.6, for no immediate slip)

a. Mode #1 response curve

b. Mode #2 response curve

Mode #2 has been optimized.

Figure #8:

a. Optimization of mode #1 for system of Figure 7. Optimized with $k_d=0.25$, $\mu N=0.225$ (Using y=9.10 for no immediate slip)

b. Optimization of mode #2 for system of Figure 7. (Replotting of Figures 6b and 7b onto similar scales.

3. HOW GRAVITY AND JOINT SCALING AFFECT STRUCTURAL RESPONSE

BY

SHYR-TZER HSU

Dept. of Mechanical Engineering

Carnegie Mellon University

Pittsburgh, PA 15213

May 12, 1987

1. INTRODUCTION

Many engineering structures are subjected to motions in which limited slip can occur between members. This is frequently the case for bolted and riveted structures and can also be the case for joints found in space applications. Truss structures designed for space often are constructed with joints that can rotate and lock into place. This allows the structure to collapse into a compact package that is easily transported to space and then expanded. Typically, this type of joint mechanism is subject to limited slip behavior because of "slop" due to machining tolerances. In addition, joint slip is usually constrained by friction forces within the mechanism. This means that the joint's motion is controlled by friction until it reaches the end of the free play and then it is constrained elastically. This type of nonlinear behavior can have a strong influence on system response. In particular because of the limited slip or the 'gap' aspect of the joint behavior scaled models of the jointed structure may not respond dynamically in the same manner as the full scale structure in space. This may be the case for two reasons.

The first reason that a scaled model of a structure may not have the same dynamic response is that tolerances in the joints are not scaled. Typically, engineers wish to have joints that behave as linearly as as possible. Consequently, when they are designing the full-scale joint they stipulate as small as tolerances as possible to reduce slop and the associated non-linear behavior. When sub-scale models of the joint are developed for testing the same absolute tolerances are stipulated since they cannot be further reduced. As a result, the free-play in the sub-scale joints is, on average, significantly greater than in full-scale joints and the model structure will exhibit stronger non-linear behavior.

A second reason that a scaled model of a structure may behave differently is that it may be tested under gravitational loading that does not occur in space. While there are laboratory procedures for supporting two dimensional structures (i.e. structures that have modes in which the motions lie in a plane) in such a way as to negate gravitational effects, they are not readily applicable to more complex, three dimensional structures. As a result, it is in general not possible to eliminate gravitationally induced preloads in the joint. The preload introduces a static displacement in the joint that tends to eliminate the free-play in one direction. Thus, for

example, the joint may behave elastically in the direction of the applied preload, and slip only when motion occurs in the opposing direction (in contrast to a joint without any static loads that slips in both directions). As a result from a dynamics point of view, a joint with preloads tends to be effectively stiffer and contributes less damping to the system. A goal of the current research is to gain a better understanding of this effect.

This research considers the dynamic response of the lumped parameter system depicted in Figure 1. The system may be viewed as either a model of a single degree of freedom oscillator or a single mode representation of a general structural system as characterized by a given modal mass, stiffness and damping. The non-linear element that represents the joint is indicated by the linkage having the spring stiffness k_d. In this linkage the friction element can slide once the magnitude of the force builds up to μN. Slip at the friction contact point is limited by the stops located at distances δ_1 and δ_2 and the total gap is given by δ. The system is subjected to a sinusoidal excitation and a static preload, f_1. This system was chosen for examination because it is the simplest system which exhibits the characteristics of interest and yet, in a modal sense, has implications to a a broad class of systems. To date we have concentrated on understanding the steady state response of this system.

The steady state response of the system is important for two reasons. The first is that it is easier to analyze than the transient response and, consequently, it is easier to establish important nondimensionalize system parameters. Since these parameters control transient response as well as steady state response the final issue is how much they change in going from a full-scale to a sub-scale system. For example, one suspects that static preloads have little effect when the system's response is large since the amount of energy dissipated by friction is then independent of the static loads. This can be readily quantified by analyzing the system's steady state response to establish for what range of dimensionless parameters this is true. This analysis is easier to perform for steady state response because well established techniques (the describing function approach) exist for determining approximate solutions. The resulting analytical solutions are superior to numerical simulations because they are easier to compute and more general. Secondly, it has been shown in other work recently performed at Carnegie Mellon (see Section 2 of this

report) that the steady state behavior of a system can be used to estimate its transient response. Thus, it is clear that gaining an understanding of the factors that control the steady state response also has a direct bearing on how it will behave in the transient regime.

Iwan has analyzed a similar limited slip system in [2]. It differs from that considered here in that it did not contain the spring with stiffness k (refer to Figure 1) nor did he consider static preloads. Both of these factors are important in space applications.

2. ANALYSIS

2.1. Formulation of Governing Equations

The equation of motion for the system shown in Figure 1 is,

$$m\ddot{x}(t)+c\dot{x}(t) + k\,x(t) = f_o\cos\omega t + f_1 - f_n(x,\delta_1,\delta_2) \qquad (1)$$

where f_1 is the static load, and f_n is the nonlinear friction force at the joint.

The contact pressure on the joint, N, is assumed constant, and the inertia of the friction element is neglected. Therefore, f_n is constant throughout the length of the friction element.

The friction element will slide once the magnitude of the nonlinear force f_n equals N multiplied by μ, the friction coefficient of the materials in contact.

The nonlinear force f_n is a function of the mass displacement x. When $|x| \le \frac{\mu N}{k_d}$, where k_d is the stiffness of the friction element, the system is linear. When $|x| \ge \frac{\mu N}{k_d}$, and the stop distances δ_1, δ_2 are sufficiently large, the system has elasto-plastic behavior. When the stop distances, δ_1 , δ_2 are not large enough, the system experiences a sudden hardening phenomenon. If the mass displacement x is periodic, several different hysteresis cycles of f_n vs. x can be drawn, as shown in Figures 2-6.

One purpose of this study is to understand the steady state response of the system shown in Figure 1. Although this task can be accomplished by solving equation (1) numerically for a sufficient long period of time; it is inefficient and computationally expensive. Therefore, an

alternate, more efficient method is developed. The direct, long time solution is then used only to verify the accuracy of the analytical results in certain representative cases.

2.2. Approximate Method

Based on the fact that the excitation is periodic; we assume that the response is also periodic. Therefore, the displacement x can be expanded by Fourier series. In the steady state, the response is approximately harmonic, i.e.

$$x = A\cos\theta + B \quad , \text{ where } \quad \theta = \omega t - \psi \tag{2}$$

In the above, the offset term B is included to compensate for the shift due to the static load f_1.

The method used here was adopted by several earlier papers [2] [3] [1] on the studies in the friction damping of structures. Since the nonlinear force f_n is excited due to the oscillation of displacement x only; it is harmonic and can be linearized by representing it in terms of a truncated Fourier series as shown below.

$$f_n = f_b + f_c\cos\theta + f_s\cos\theta \tag{3}$$

Where

$$\begin{aligned} f_b &= \mu N F_b(\alpha, \beta, \gamma, q) \\ f_c &= \mu N F_c(\alpha, \beta, \gamma, q) \\ f_s &= \mu N F_s(\alpha, \beta, \gamma, q) \end{aligned} \tag{4}$$

In the above, F_b, F_c, F_s are nondimensioned Fourier coefficients established in the Appendix and α, β, γ and q are dimensionless parameters also established in the Appendix (see equation (34)).

It is noted that since the dynamic displacement is proportional to $\cos\theta$, it is apparent from equation (3) that f_c contributes to the dynamic stiffness of the system while f_s provides damping. The stops shown in Figure 1 suddenly contribute to the elements stiffness and significantly inhibits joint damping. As can be seen in Figure 7, f_s decreases with the amplitude right after the limit stops are hit.

To obtain the approximate solution, equations (2) and (4) are substituted into equation (1).

After equating the linearly independent terms, phase shift ψ is eliminated by using the relation $\sin^2\psi + \cos^2\psi = 1$. Then the following two nonlinear algebraic equations are obtained.

$$kB + f_b - f_1 = 0. = g_1(A, B, \omega) \tag{5}$$

$$[(k - m\omega^2)A + f_c]^2 + [\omega cA - f_s]^2 - f_o^2 = 0. = g_2(A, B, \omega) \tag{6}$$

Equations (5) and (6) are solved iteratively to get the frequency response of the vibratory amplitude A and the permanent offset B.

2.3. Calculation of Peak Response

By holding the system parameters constant, the peak vibratory amplitude A is obtained as

$$\frac{\partial A_m}{\partial \omega_m} = 0. \quad \text{at} \quad \omega = \omega_m \tag{7}$$

To relate equation (7) with equations (5) and (6), it is observed that A and B are both functions of ω. Consequently, g_1 , g_2 are only functions of ω, and

$$\frac{dg_1}{d\omega} = \frac{\partial g_1}{\partial A}\frac{\partial A}{\partial \omega} + \frac{\partial g_1}{\partial B}\frac{\partial B}{\partial \omega} + \frac{\partial g_1}{\partial \omega} = 0. \tag{8}$$

$$\frac{dg_2}{dg_1} = \frac{\partial g_2}{\partial A}\frac{\partial A}{\partial \omega} + \frac{\partial g_2}{\partial B}\frac{\partial B}{\partial \omega} + \frac{\partial g_2}{\partial \omega} = 0. \tag{9}$$

From equation (5), we know $\partial g_1 / \partial \omega = 0.$, and from equation (7) , we have

$$\frac{\partial g_1}{\partial B}\frac{\partial B}{\partial \omega} = 0. \quad \text{and} \quad \frac{\partial g_1}{\partial B} = k \neq 0. \tag{10}$$

It implies,

$$\frac{\partial B}{\partial \omega} = 0. \quad \text{at} \quad \omega = \omega_m \tag{11}$$

Consequently, from equation (9), we have

$$\frac{\partial g_2}{\partial \omega} = \{ c [\omega cA - f_s] - 2 m\omega [(k - \omega^2 m)A + f_c] \}(2A) = 0. \quad \text{at} \quad \omega = \omega_m \tag{12}$$

Thus, the three equations that determine the peak values A and B at the corresponding resonant frequency of excitation are

$$
\begin{aligned}
& g_1(A_m, B_m, \omega_m) = 0. \\
& g_2(A_m, B_m, \omega_m) = 0. \\
& \frac{\partial g_2}{\partial \omega}(A_m, B_m, \omega_m) = 0.
\end{aligned}
\tag{13}
$$

To solve equation (13), it is noted that equation (5) is decoupled from equations (6) and (12). And from the relation (6) + (12)ω = 0, we have

$$F\omega_m^4 + G\omega_m^2 + H = 0. \tag{14}$$

where

$$
\begin{aligned}
F &= 5(mA_m)^2 \\
G &= 3\{(c^2 - 2mk)A_m^2 - 2mA_m f_c\} \\
H &= (kA_m)^2 + f_c^2 + 2kA_m f_c + f_s^2 - f_o^2
\end{aligned}
\tag{15}
$$

By plugging equation (12) into equation (6), we have

$$\{\omega_m c A_m - f_s\}^2\{1 + (\frac{c}{2m\omega_m})^2\} = f_o^2 \tag{16}$$

Therefore, from equations (13),(14), (15) and (16), the following iterative equations for calculating the peak response can be obtained

$$
\begin{aligned}
B_m &= \frac{f_1 - f_b}{k} \\
A_m &= \{f_s - |f_o| / \sqrt{1 + (c/2m\omega_m)^2}\} / c\omega_m \\
\omega_m &= \{(\frac{1}{2F})(-G + \sqrt{G^2 - 4FH})\}^{\frac{1}{2}}
\end{aligned}
\tag{17}
$$

To solve equation (17), group values of (A_m, B_m, ω_m) are first initialized to calculate the Fourier coefficients f_b, f_s, f_c. Iterations are then made utilizing equation (17) until (A_m, B_m, ω_m) converge.

3. NUMERICAL RESULTS

3.1. Frequency Response

To examine the validity of the approximate method; equation (1) is solved directly using the Runge-Kutta method. The steady state response is then obtained from the "long time" transient solution. The results are compared with the ones calculated by the approximate method. These comparisons are plotted in Figures 8-12 , in which the discrete symbols denote the transient solutions. These figures show that a good agreement exists between the two approaches.

In Figure 8, the influence of gap length δ on the vibratory amplitude frequency response is shown. For $\delta=0.$, the system is linear. For $\delta \to \infty$, the friction joint is dominated by the friction damping, and system behaves plastically. In between, a transition region exists for a certain range of δ values, where the system shifts from elastic to plastic behavior. In this region, the vibratory amplitude A may become multi-valued at some fixed excitation frequencies. This phenomenon is typically referred to as "unstable response". A typical case for $\delta=20.$ is shown in the figure.

Unstable response can also be seen in Figure 9, in which the amplitude is calculated for several different values of the normal load μN. For $\mu N = 1.0$ and 2.0, the system responses are stable (vibratory amplitude is single valued). For $\mu N = 1.5$, unstable behavior is clearly seen. The physical explanation of this behavior is that at low μN value, the friction damping has little effect on the system response which is primarily dominated by the constant stiffnesses k, k_d and the system behaves linearly. For high μN values, the friction element is partially stuck due to the stronger friction resistance. Under this condition, neither of the limit stops is hit during the motion cycle. As a result the energy dissipation per cycle remains constant for each fixed excitation frequency, and the system response is stable. For normal load in the median range, as the case of $\mu N = 1.5$ shown in the figure, the limit stops are hit by the element during the motion cycle. The system response becomes meta-stable or unstable. This is due to the fact that the energy dissipated by friction per cycle remains constant while, because of the limit stops, the element stiffness significantly increases with amplitude. This results in the multi-valued response indicated in Figure 9.

Multi-valued behavior is also seen in Figure 10; where the amplitude is calculated for various stiffness ratios k_d / k. A region of unstable behavior is seen for $k_d / k = 0.25$, where a disconnected closed curve occurs. The appearance of disconnected regions in this more general system model agree well with Iwan [2]'s earlier work.

The effect of static load f_1 on the vibratory amplitude frequency response is shown in Figures 11 and 12. Since the energy dissipation per cycle depends on the excitation and damping only, it remains the same after the static load is applied to the system. However, the static load causes a permanent offset, which is represented by the symbol B as is shown in equation (2). Under high excitation force f_o at resonant frequency, both limit stops shown in Figure 1 are hit during the motion cycle , and the offset has little effect on the vibratory amplitude. However, at some off-resonant frequencies, the response is sufficiently low that there is a difference in the response since without the static preload the limit stops would not be encountered during the motion cycle. However, once the static load is applied, the permanent offset thus generated adds to the dynamic displacement and causes the friction element to hit one of the stops and affects the dynamic response.

Based on the above argument, it is then understandable that the static load may even raise the maximum amplitude of the system under low excitation force f_o. This fact is depicted in Figure 12 where the maximum amplitude is increased when the static load $f_1 = 10$.

Consequently, under certain conditions static preload can have a significant effect on vibratory response. For some excitation, the presence of a large static load may even eliminate the multi-valued response and stabilize the system. For a large structure to be used in space, this means that because of gravitational effects it may not be possible to duplicate on earth the actual response that might occur in space. Therefore, this effect needs to be carefully analyzed in order to properly interpret laboratory test data and predict the response of the full-scale structure in space.

3.2. Peak Amplitude Response

First consider the system's response when there are no stops to limit slip in the nonlinear element. The amplitude of peak response will then depend on how stiff the nonlinear spring (relative to the system's stiffness, k) and the value of the slip load, μN. Some representative results are presented in Figure 12. For sufficient large μN, the friction element is stuck and the system is linear. This is also the case when $\delta = 0$. The system is also behaves linearly when μN is zero since no energy is dissipated by friction. It can be seen from the plot that the friction damping effect is only significant for μN between 0 and some maximum value, μN_{max}. Furthermore, a minimum peak vibratory amplitude exists for a certain μN value, as shown in the figure. This fact has been discovered and experimentally verified by Griffin[3].

Figure 14 shows the plot of resonant frequency vs. normal load μN at gap length $\delta = \infty$. It is observed that resonant frequency increases with the normal load, and hits a maximum when the normal load is sufficiently large that the friction element is always stuck. Again this indicates that the effect of normal load is only significant over a finite range.

The effect of gap length on the peak vibratory amplitude response is indicated by the results depicted in Figure 15. A plot of the resonant frequency vs. gap length is given in Figure 16. In both figures, the γ at the abscissa denotes the nondimension gap length defined in equation (34). In both plots it can be seen that for μN, a transition region exists in which the gap length strongly affects the dynamic response. For gaps larger than a certain value, the limit stops shown in Figure 1 will no longer limit slip in the friction element and, consequently, further increases in gap length will not affect the resonant response. It is clear that the gap length effect is only significant in the transition region. This is depicted in Figures 17-18, which are the scaled versions of the Figures 15-16. The critical gap length δ_{cr} is defined as the value beyond which the resonant response is unchanged. This value is determined through numerical experiments for different system parameters, and is used as the scale length in the abscissa for both plots.

At $\delta=0$ the system resonant response is dominated by stiffness and viscous damping. At $\delta=\infty$, the system resonant response depends on the stiffness, and both viscous and friction

damping. The difference between the two responses is used to scale the results in Figures 17 and 18.

Since the resonant response is only affected by the normal load $\mu N = 0$ to μN_{max}, the results for different normal loads all lie fairly closely together in a band as indicated in Figure 17 for amplitude and Figure 18 for frequency. It was shown in Figure 13, that the lowest resonant response comes at a specific μN value (0.1 for the system consider here) and this case provides a lower bound on the response when the data is depicted as in Figure 17. The normal loads which are greater or less than this value then approach this common lower bound of the band.

In Figure 18 the curve for $\mu N = 5.0$ stands out as unusual. Addition work is being done to check this result and, if it is correct, to further understand the physical basis of this behavior.

As the normal load goes to zero or when it approaches N_{max} the system becomes linear and the stiffness has no effect on the lower bound curve of the band. However, an increase in the element's stiffness k_d/k can affect the upper bound of the curves. This is shown in Figures 19 and 20 for resonant amplitude and frequency respectively.

4. CONCLUSION

The approximate solution method based on a describing function approach has been verified to be an effective tool in studying the response of system containing a friction joint with limited slip. It is believed that this approach could be extended to investigate the steady state response of a large truss-like jointed structure and utilizing the procedures discussed in Section 2 could be used to calculate transient response.

It has been found that under certain conditions the vibratory amplitude of the system may become multi-valued at certain excitation frequencies. A large jointed structure may have significant variations in the joint properties from joint to joint due to machining differences. As a result some of the joints may experience the conditions that lead to multi-value response. Consequently, it may be difficult to get repeatable experimental results since the structure may

settle into different patterns of response depending on fairly subtle aspects of how the loads are applied. The difficulty is intensified for laboratory tests of sub-scaled models of space structures since the scatter in the joint's free-play is relatively larger (with respect to the smaller dimensions of the model joint).

This work also shows that in some circumstances, the presence of static preloads may significant affect the system's dynamic response. In this case if a large structure is ground tested it may be necessary to first correlate the data with an analytical model of the structure that includes preload effects. Then eliminate the preloads in the model and predict its behavior in space.

Lastly, a way of looking at system response in terms of non-dimensionalized joint properties has been developed. These curves are useful because they indicate how sensitive a system is to changes in joint tolerances. When one makes a scale-model of a joint the relative tolerances and free-play in the joint increase. The computed results indicate an approach for assessing system sensitivity to such changes.

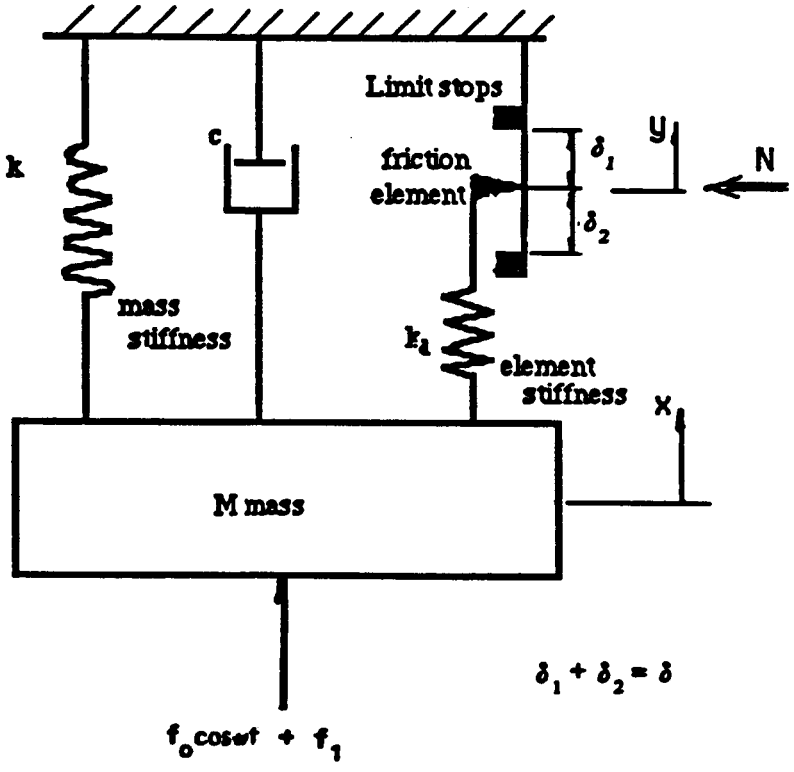

Figure 1: Single Degree of Freedom System with a Limit Slip Joint

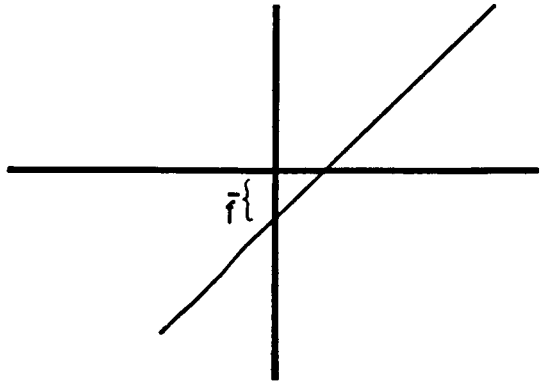

Figure 2: Non Slip

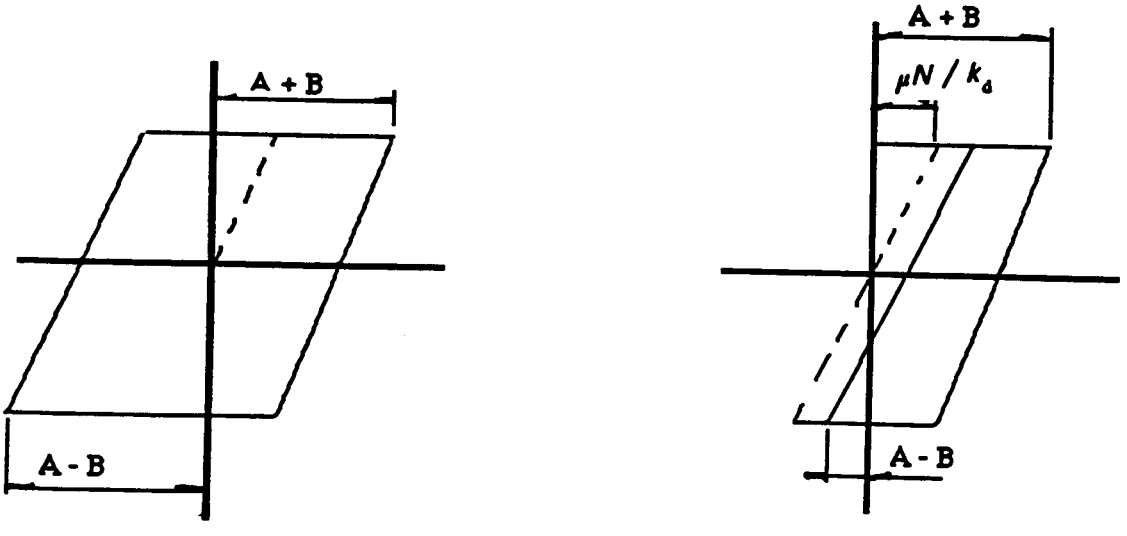

Figure 3: Pure Slip

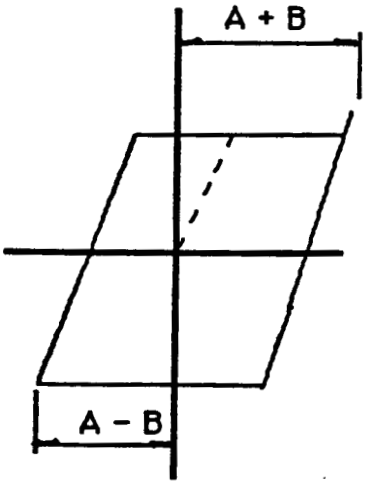

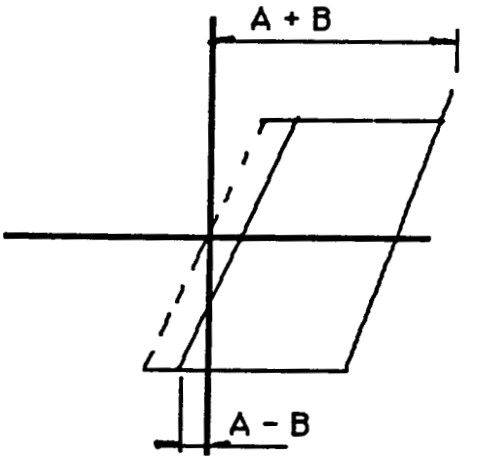

Figure 4: Slip with Upper Limit

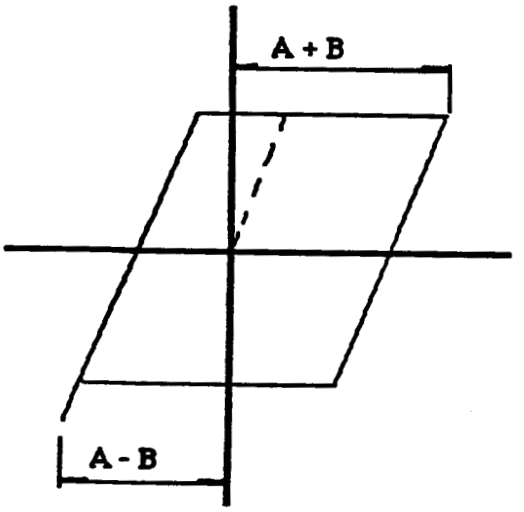

Figure 5: Slip with Lower Limit

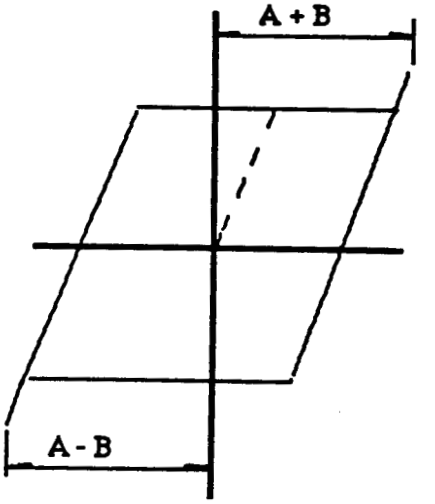

Figure 6: Slip with both Limits

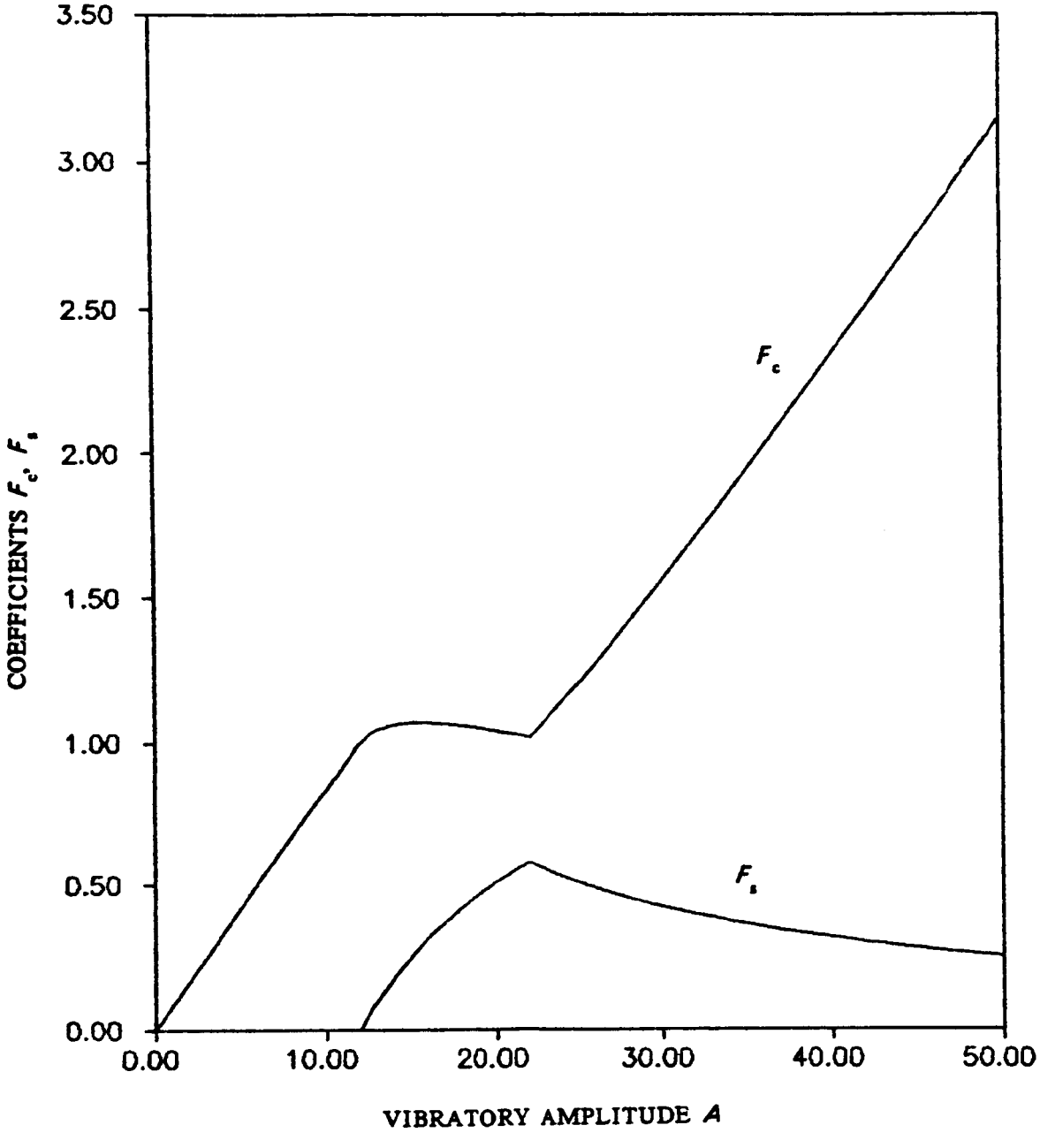

Figure 7: Fourier Coefficients f_s, f_c vs. Vibratory Amplitude A , δ=20.

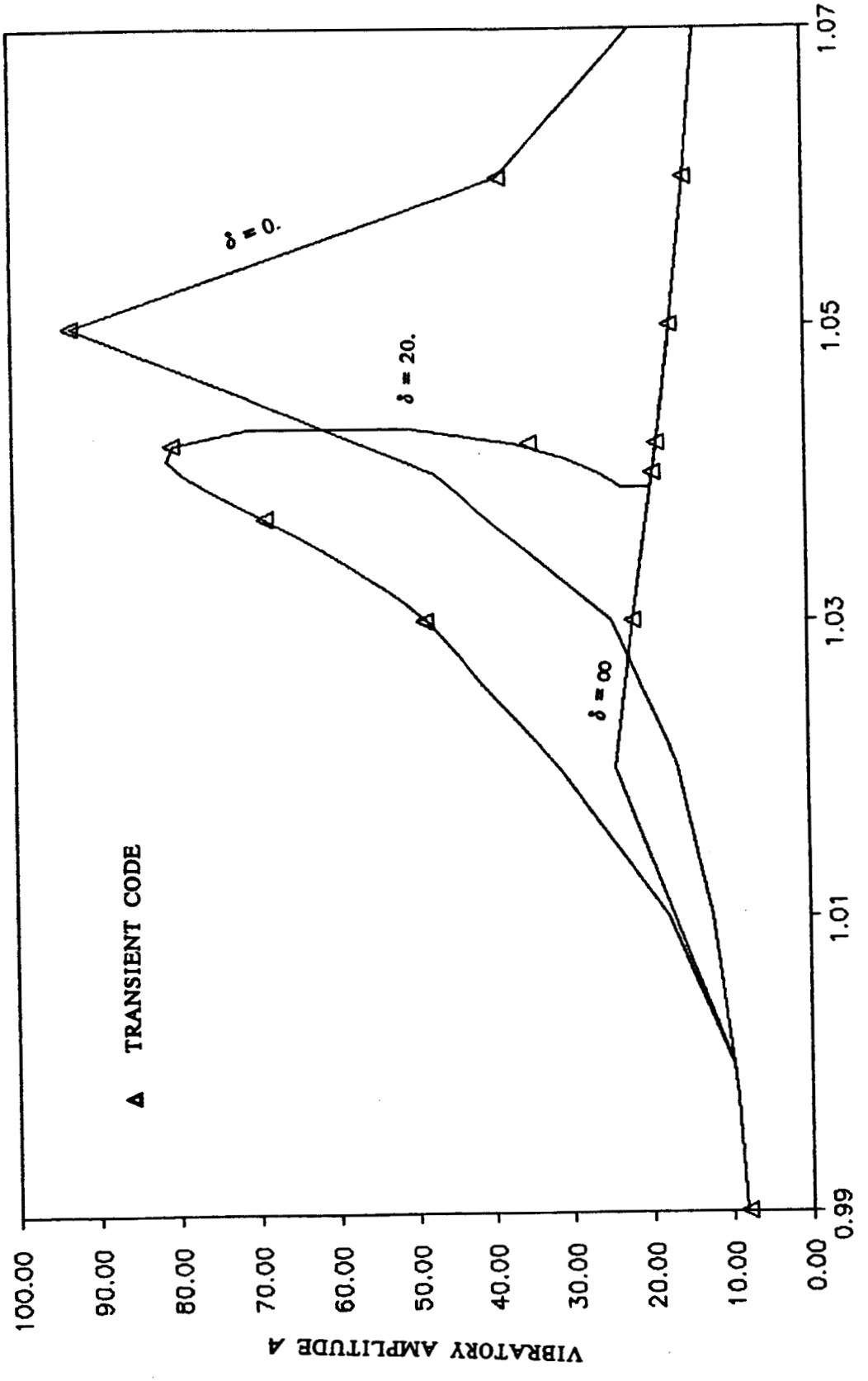

Figure 8: Vibratory Amplitude vs. Frequency with Varied Gap Length δ, f_o=1, f_1=0., m=1.,c =0.01, k_d / k = 0.1, μN = 1.0, q = 0.5

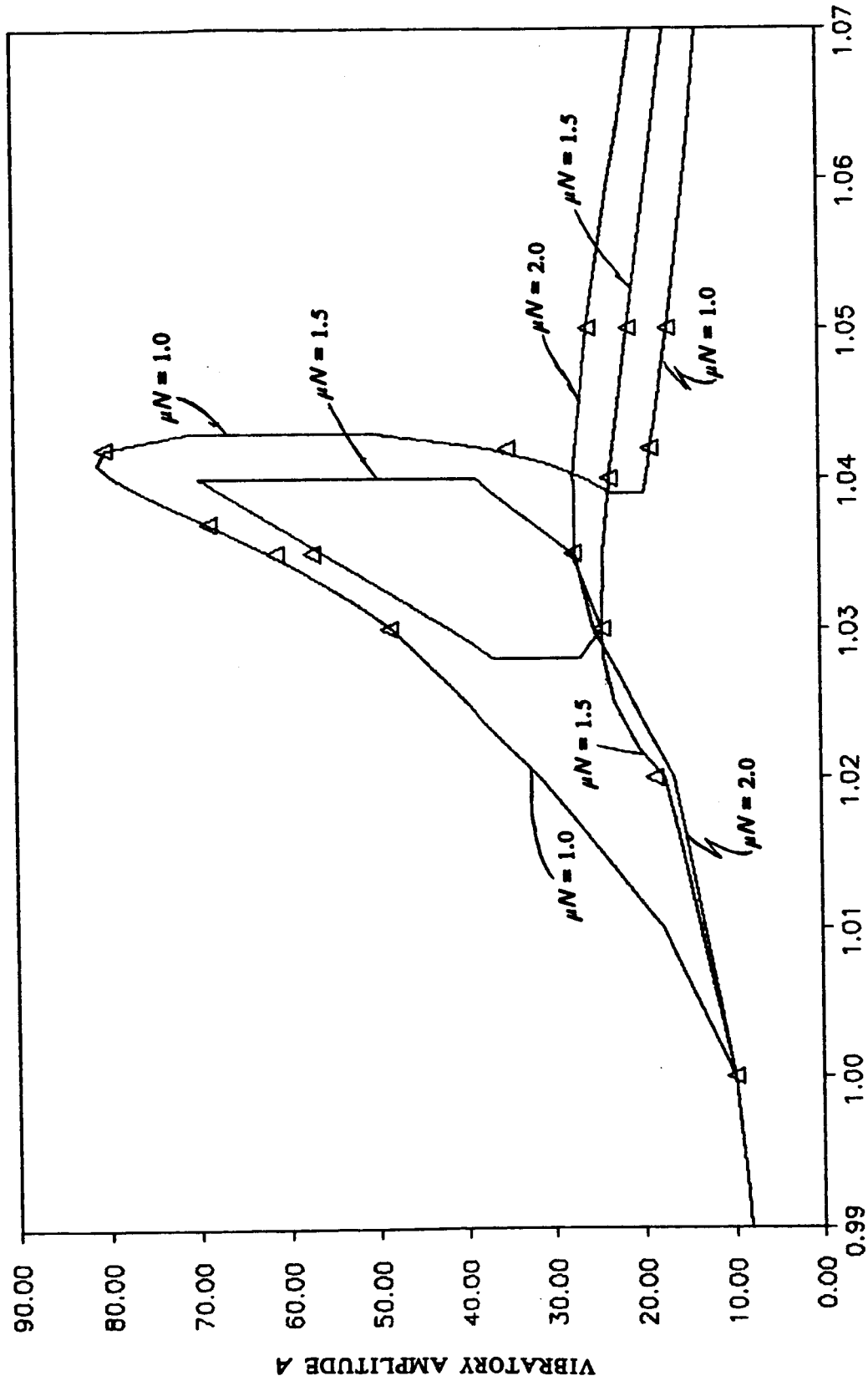

Figure 9: Vibratory Amplitude vs. Frequency with Varied Normal Load μN, f_o=1.0, f_1=0., m = 1., c = 0.01, k_d/k = 0.1, δ=20., q=0.5

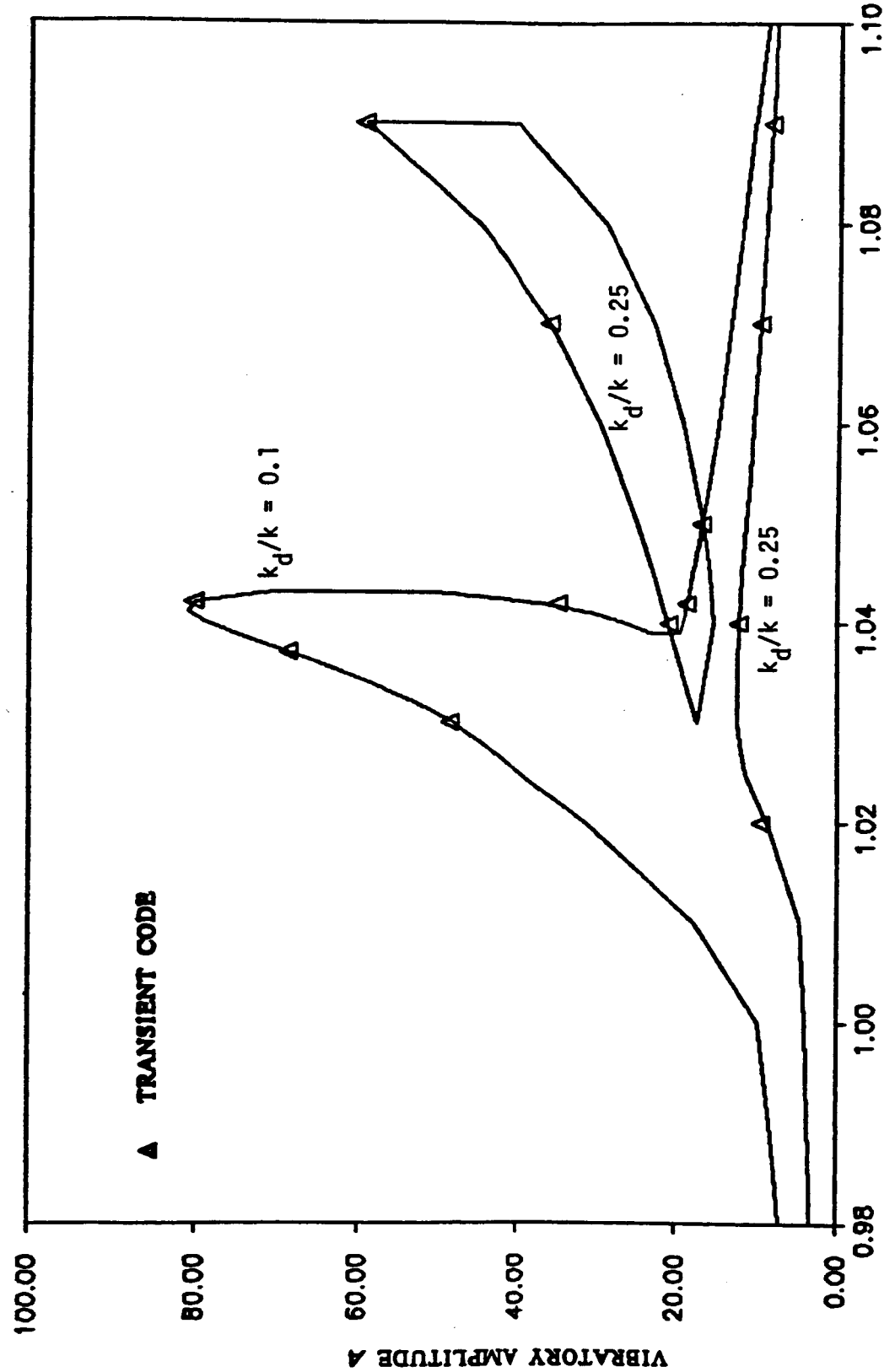

Figure 10: Vibratory Amplitude vs. Frequency with Varied Stiffness k_d/k, f_o=1.0, f_1=0., m = 1., c = 0.01, μN=1.0, δ=20., q = 0.5

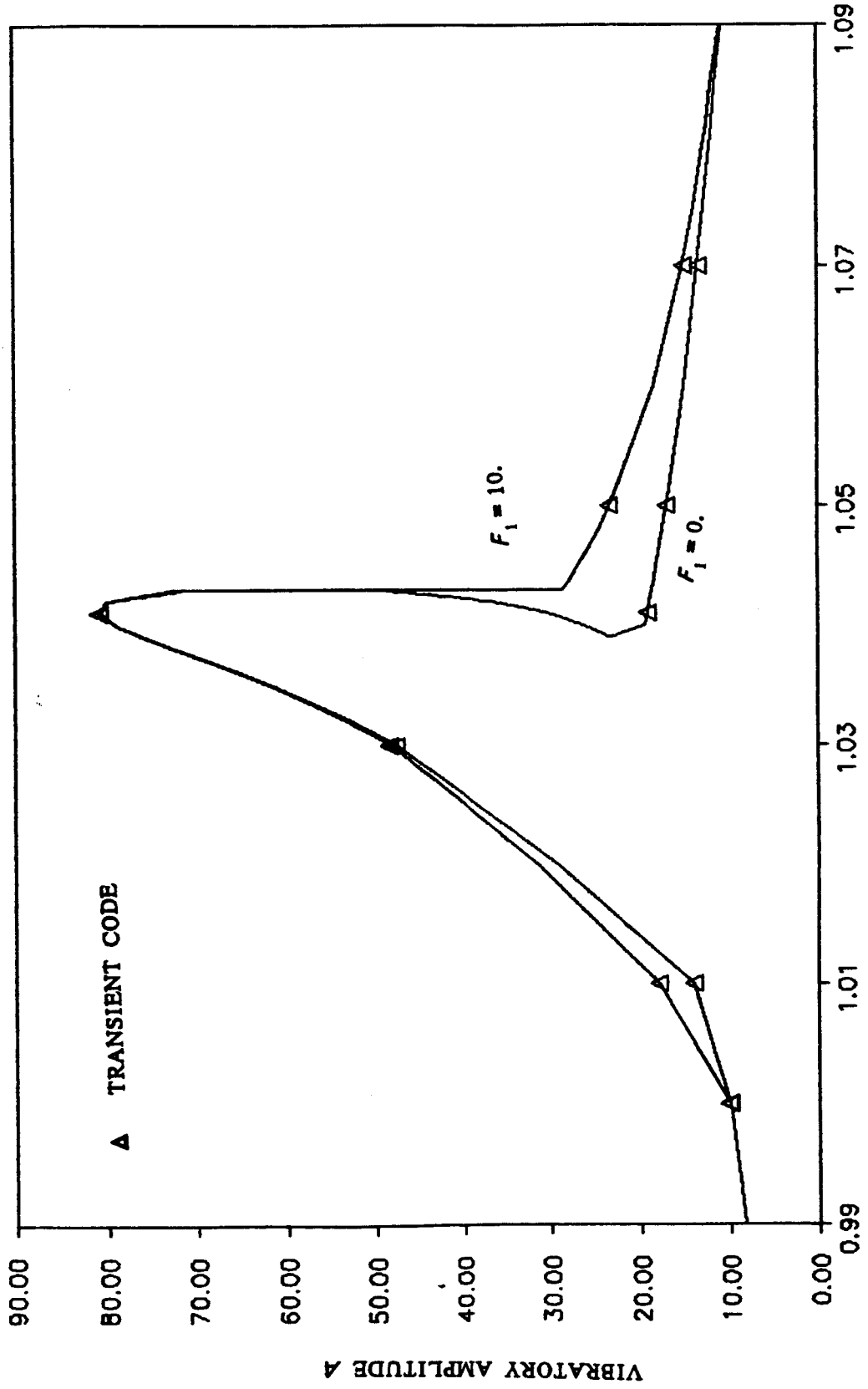

Figure 11: Static Load on Amplitude Frequency Response Under High Excitation, f_o=1., m=1, c=0.01,k_d/k=0.01, μN=1.0. δ=20.,q = 0.5

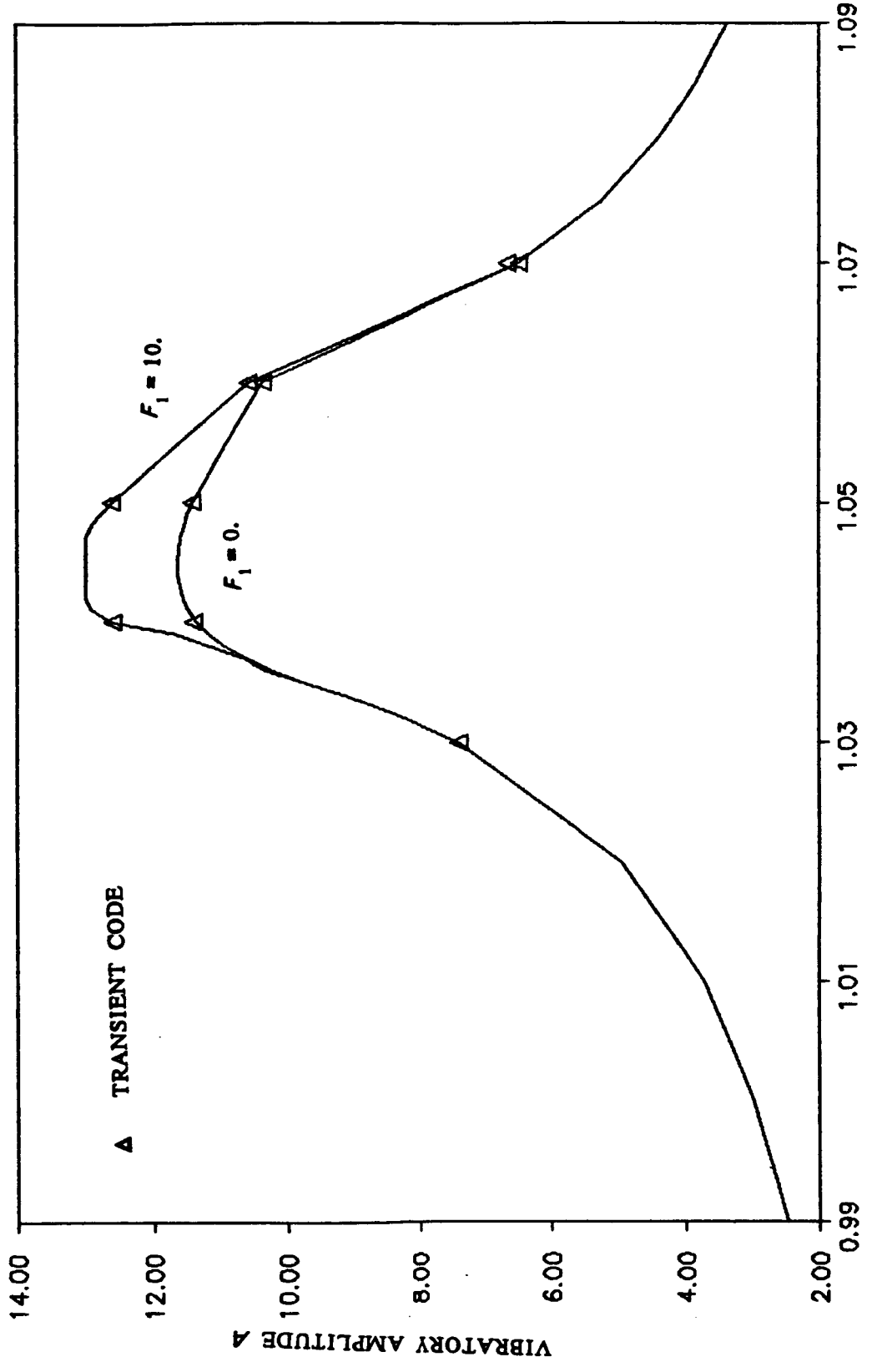

Figure 12: Static Load on Amplitude Frequency Response Under Low Excitation, f_o=0.3, m=1., c=0.01,k_d/k=0.01, μN=1.0, δ=20., q = 0.5

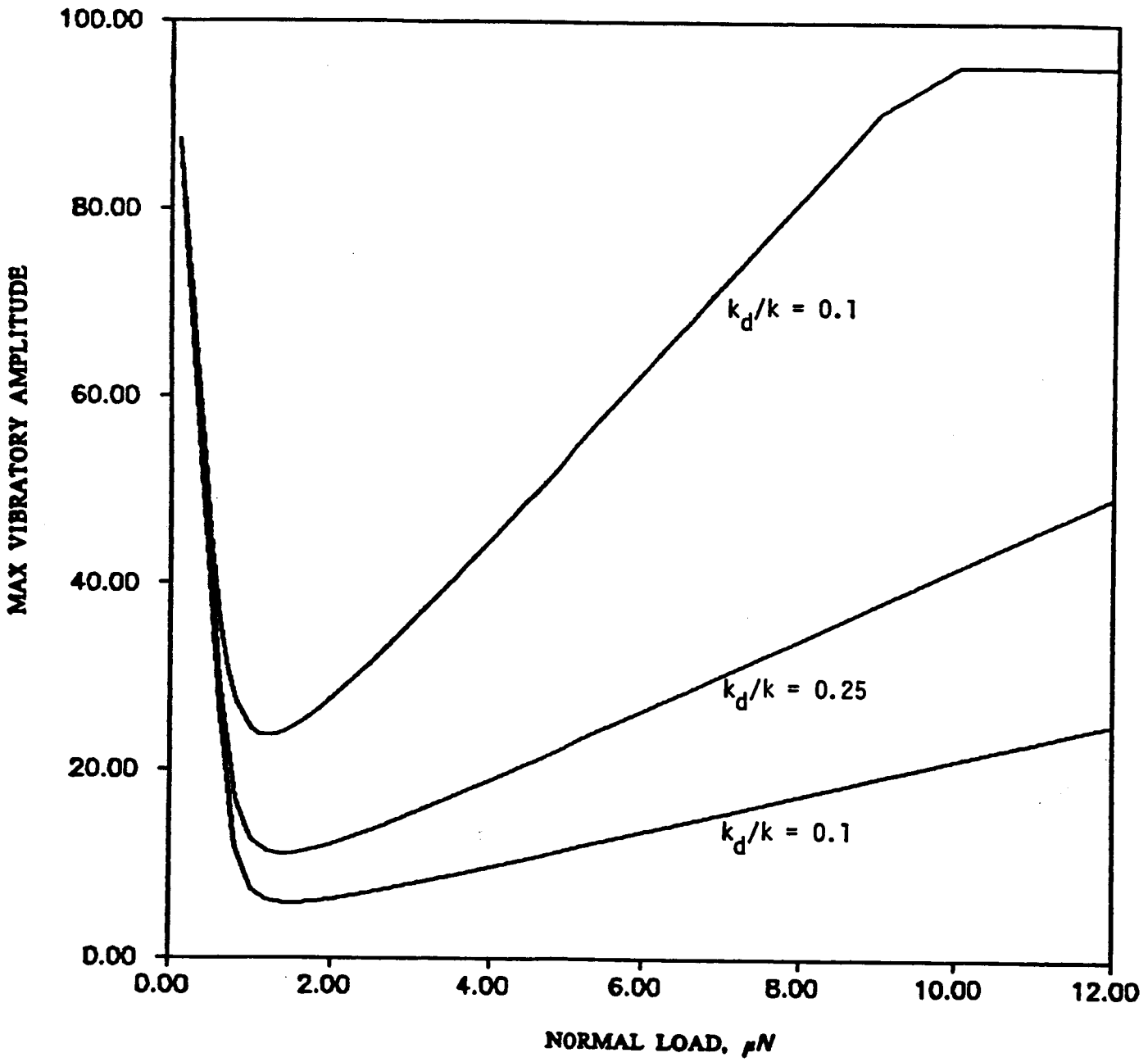

Figure 13: Max. Vibratory Ampiltude vs. Normal Load μN when Gap Length $\delta = \infty$, $q = 0.5$

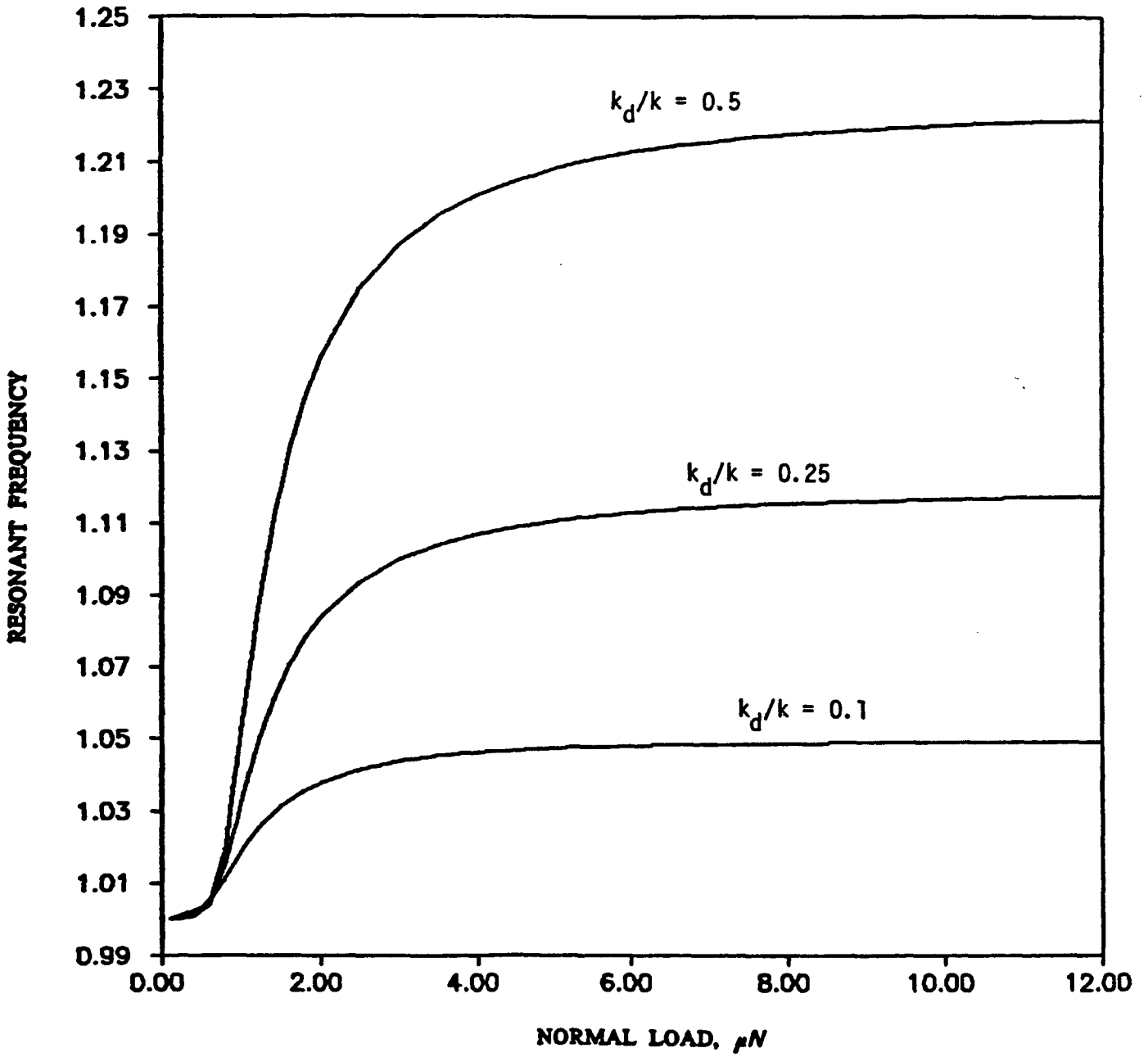

Figure 14: Resonant Frequency vs. Normal Load μN when Gap Length $\delta = \infty$, $q = 0.5$

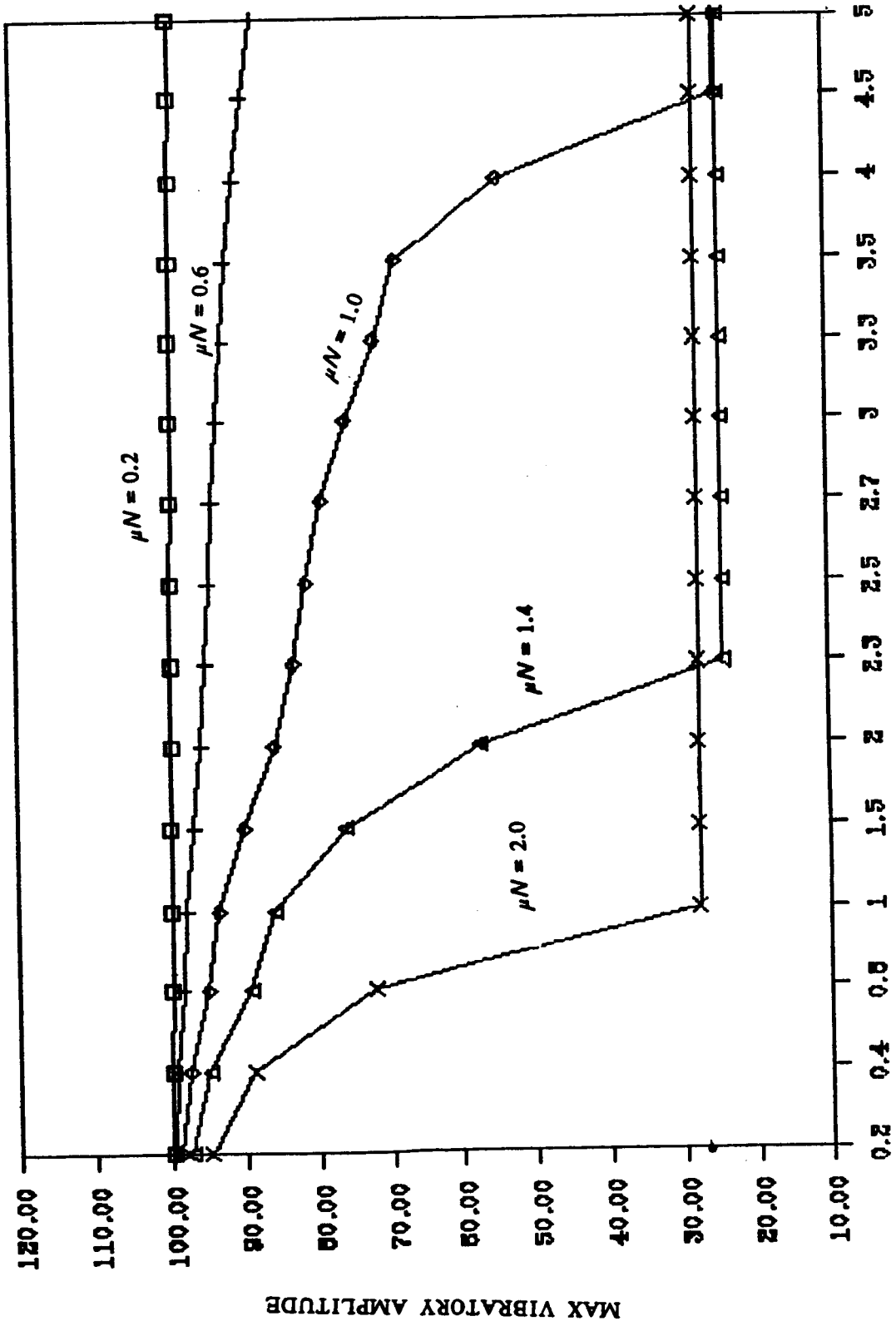

Figure 15: Max. Vibratory Amplitude vs. γ , q = 0.5

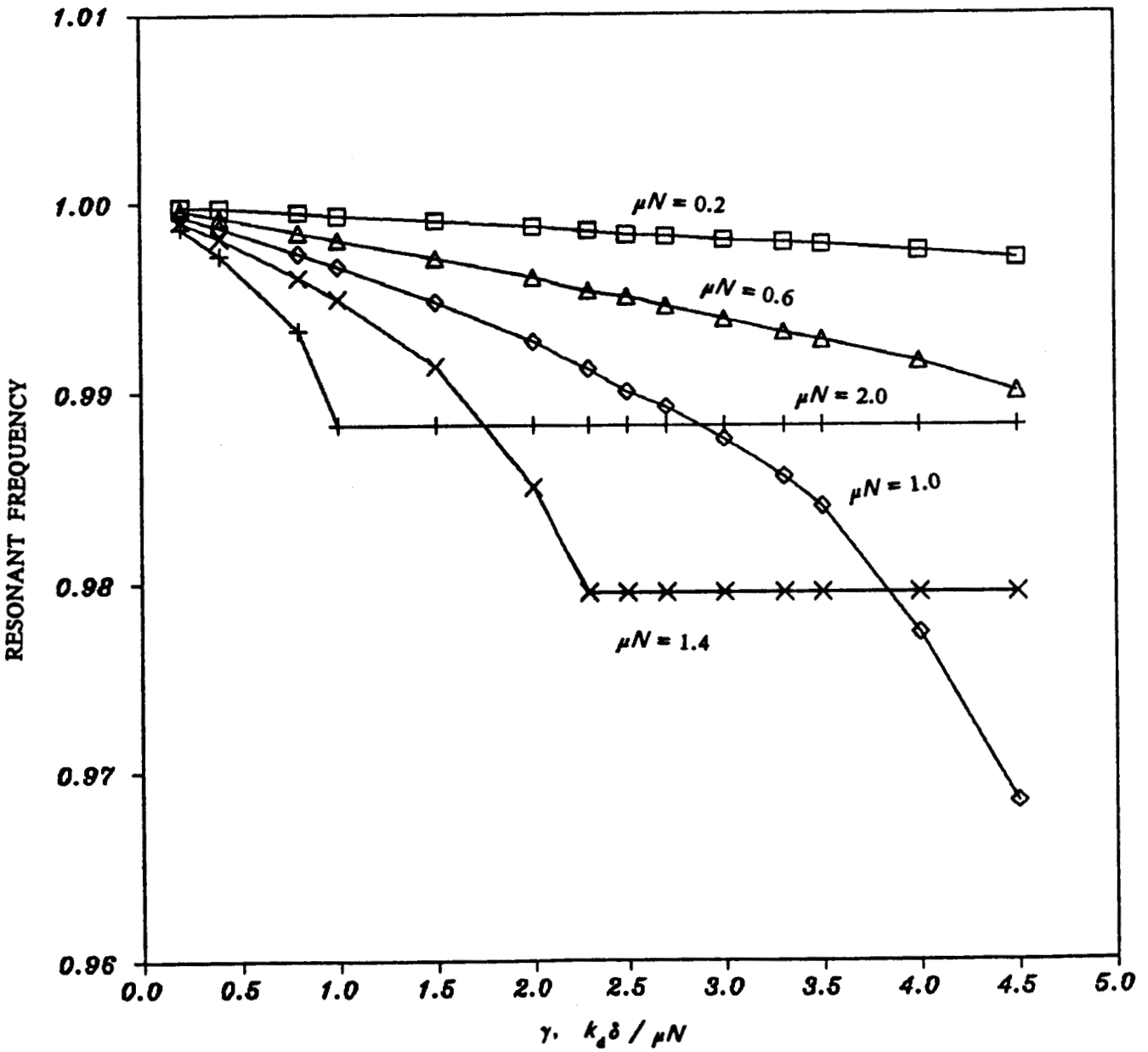

Figure 16: Resonant Frequency vs. γ, $q = 0.5$

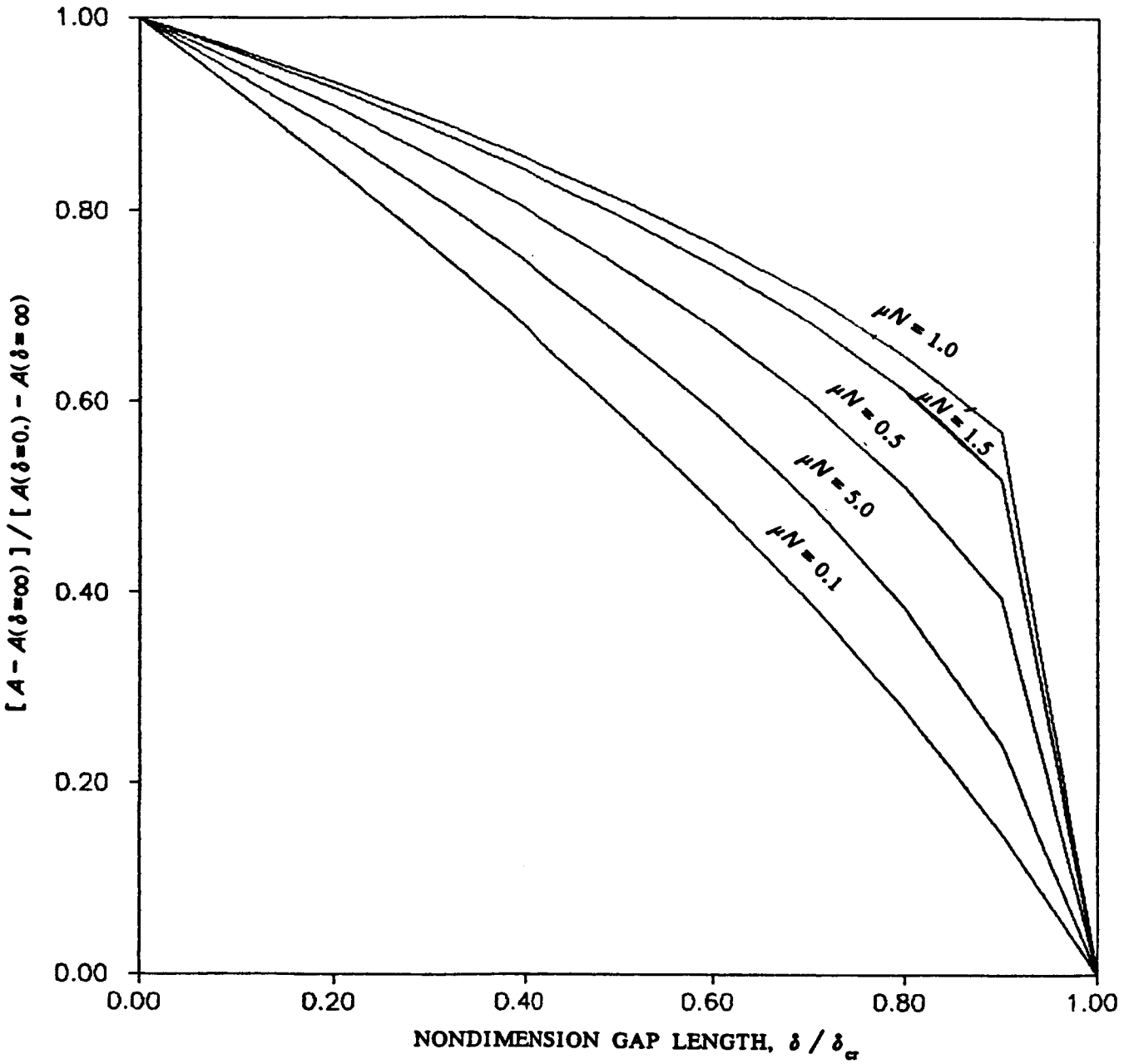

Figure 17: Scaled Max. Amplitude vs. δ/δ_{cr} with Varied Normal Load μN, $q = 0.5$

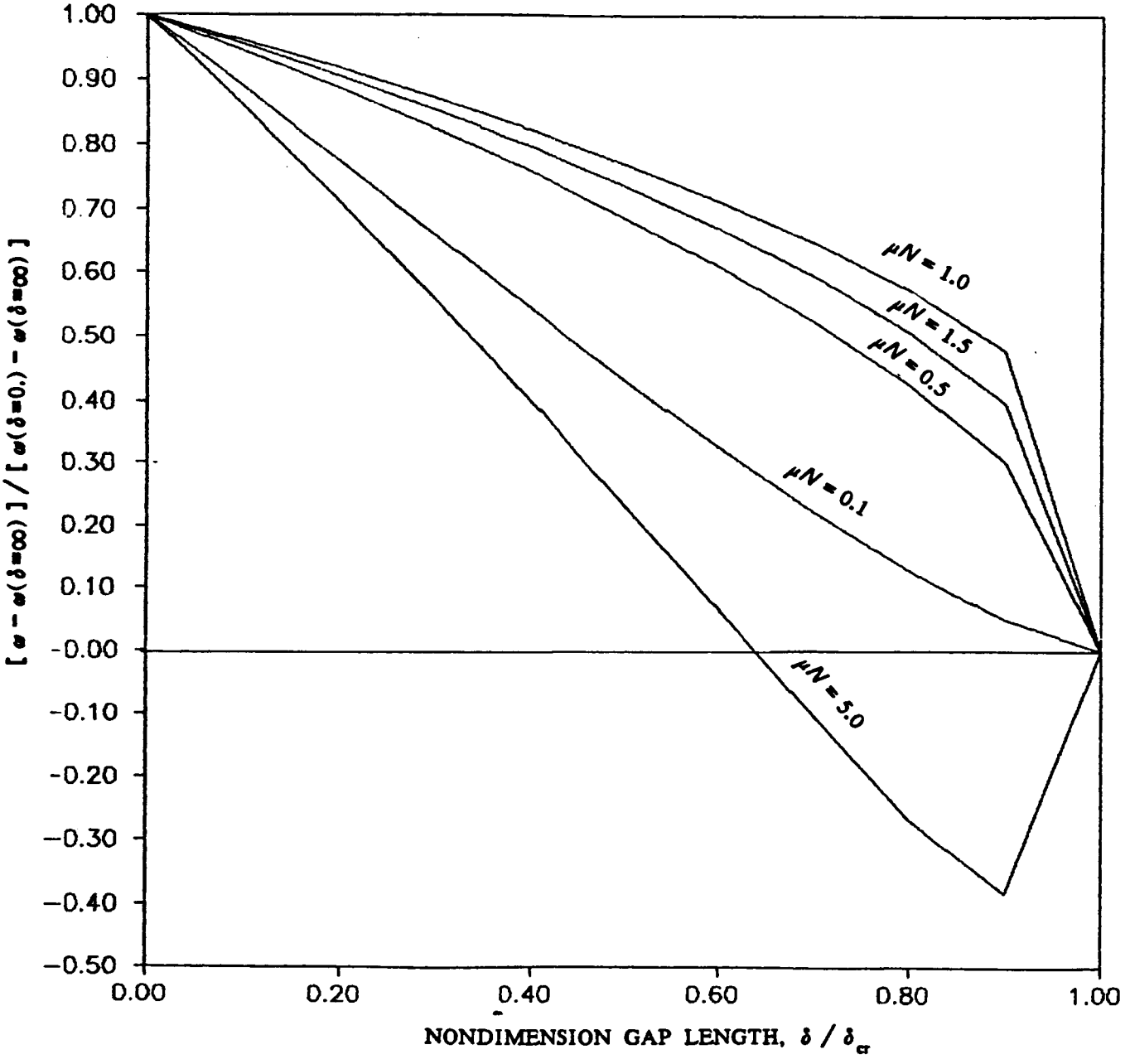

Figure 18: Scaled Resonant Frequency vs. δ/δ_{cr} with Varied Normal Load μN, $q = 0.5$

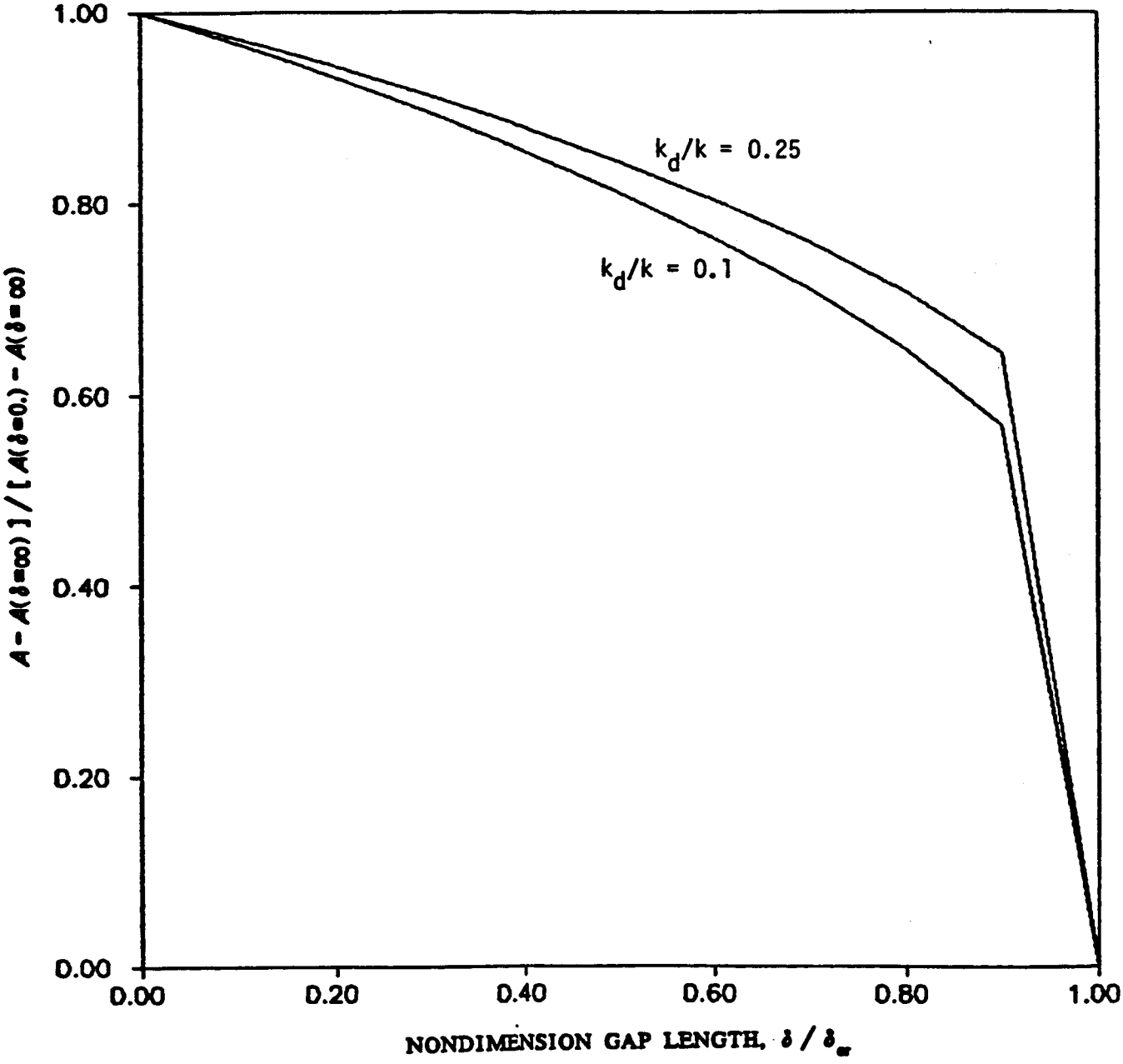

Figure 19: Scaled Max Amplitude vs. δ/δ_{cr} with Varied Stiffness k_d/k, $q_- = 0.5$

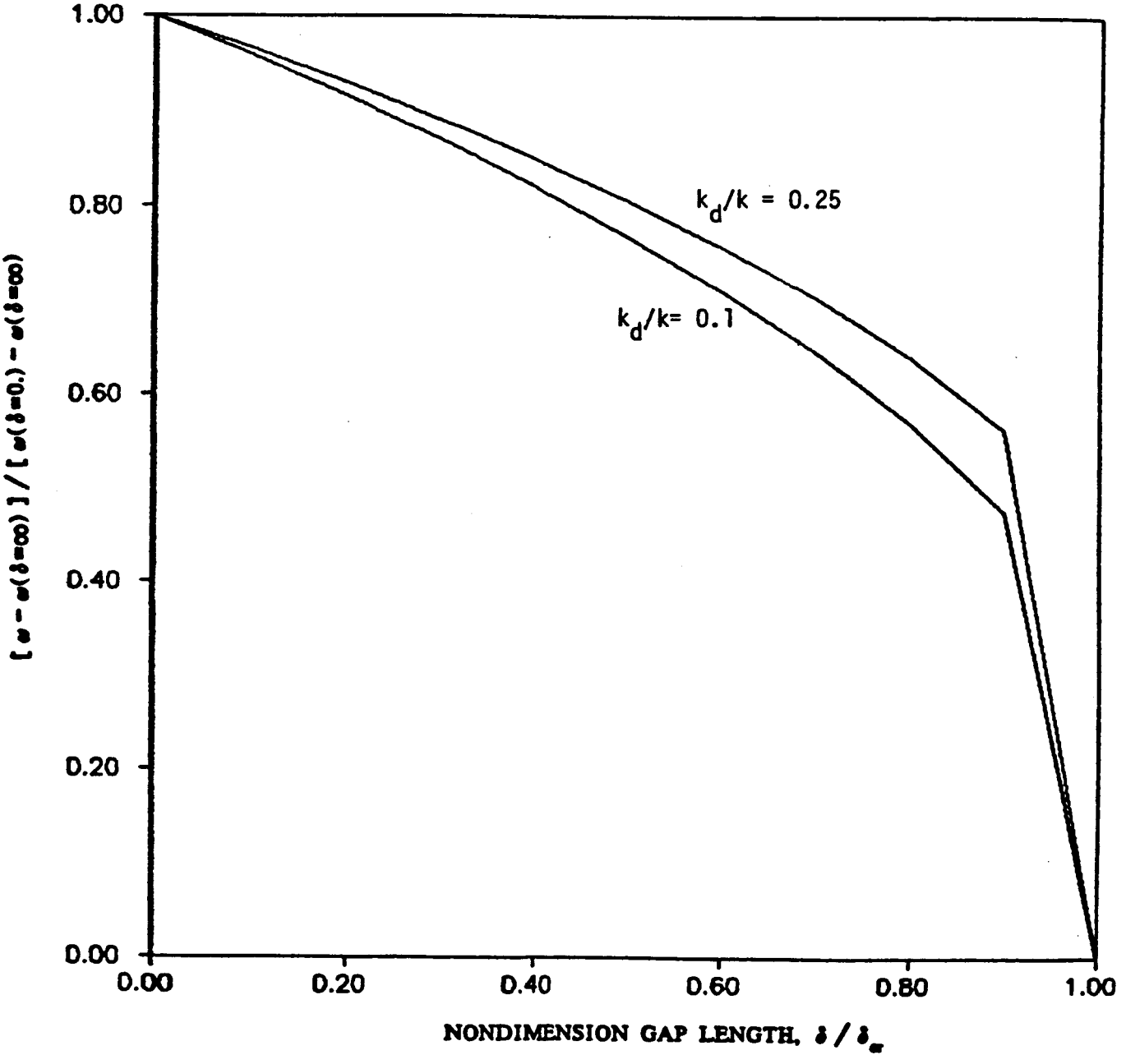

Figure 20: Scaled Resonant Frequency vs. δ/δ_{cr} with Varied Stiffness k_d/k, $q = 0.5$

I. APPENDIX : Calculation of Fourier Coefficient of Nonlinear Force f_n

The variations of the nonlinear friction force f_n is considered as follows:

The friction contact sticks initially, and f_n varies linearly with slope k_d. When $f_n = \pm \mu N$, it starts to slide , and f_n remains constant until the displacement x achieves an extremum or the friction contact hits either one of the stops. In the latter case, f_n again varies linearly with slope k_d until x achieves an extremum.

When the mass reverses direction, force f_n first decreases linearly to its original $\pm \mu N$ value and sticks again. The above process is then repeated in the opposite direction.

Given this behavior, the nonlinear force can therefore be expanded as a function of the mass displacement during a cycle of oscillation. The Fourier coefficients can then be calculated in terms of the amplitude of vibration.

The displacement is assumed sinusoidal plus a D.C. offset, i.e. $x = A\cos\theta + B$. Based on this, five different cases can be concluded. These results are summarized in the following sections.

Case 1. No slip : $0. \le A+B \le \frac{\mu N}{k_d}$,and $0. \le A \le \frac{\mu N}{k_d}$

For this case, an unknown slip may occur during the transient response which results in a permanent offset at the steady state. This causes an equally unknown value of a friction force as the $\bar{f}$ shown in Figure 2. Along with the contribution of D.C. offset B , coefficient f_b is $f_b = k_d B - \bar{f}$. However, f_b is limited between these values.

$$k_d - \mu N \le f_b \le \mu N - k_d A \tag{18}$$

And

$$f_c = k_d A$$
$$f_s = 0.$$

Case 2. Pure slip : $\frac{\mu N}{k_d} \le A+B \le \delta_1 + \frac{\mu N}{k_d}$, $A-B \le \delta_2 + \frac{\mu N}{k_d}$ and $A \ge \frac{\mu N}{k_d}$

This is the case when both the stop distances δ_1, δ_2 are sufficiently large; hence slip is

not hindered. From Figure 3, the friction force can be divided into four sections during a displacement cycle.

$$f_n = \begin{cases} (\mu N - k_d A) + k_d A\cos\theta & , 0. \le \theta < \theta_1 \\ -\mu N & , \theta_1 \le \theta < \pi \\ (k_d - \mu N) + k_d A\cos\theta & , \pi \le \theta < \theta_2 \\ \mu N & , \theta_2 \le \theta \le 2\pi \end{cases} \tag{19}$$

Where

$$\theta_1 = \cos^{-1}\{\, 1. - \frac{2\mu N}{k_d A}\}$$

$$\theta_2 = 2\pi - \cos^{-1}\{\, \frac{2\mu N}{k_d A} - 1.\,\} \tag{20}$$

It is observed that the D.C. offset B has no effect on the nonlinear force f_n in this case. Using equations 18 and 19, the nonlinear force f_n can be expanded by Fourier series as

$$f_n = f_c\cos\theta + f_s\sin\theta \tag{21}$$

Where

$$f_b = 0.$$

$$f_c = \frac{1}{\pi}\{(2\mu N - k_d A)(\sin\theta_1 - \sin\theta_2) + \frac{k_d A}{2}(\theta_1 + \theta_2 - \pi) + (\frac{k_d A}{4})(\sin 2\theta_1 + \sin 2\theta_2)\} \tag{22}$$

$$f_s = \frac{1}{\pi}\{(2\mu N - k_d A)(\cos\theta_2 - \cos\theta_1) - 2k_d A + (k_d A)(2. - \cos 2\theta_1 - \cos 2\theta_2)/4.\,\}$$

Case 3. Slip with upper Limit : $A + B \ge \delta_1 + \frac{\mu N}{k_d}$, $A - B \le \delta_2 + \frac{\mu N}{k_d}$, and $A \ge \frac{\mu N}{k_d}$

In this case (Figure 4), the upper stop is hit during the displacement cycle. Again, the nonlinear force can be separated in five sections, as shown below

$$f_n = \begin{cases} k_d(B - \delta_1) + k_d A\cos\theta & , 0. \le \theta < \theta_1 \\ -\mu N & , \theta_1 \le \theta < \pi \\ (k_d A - \mu N) + k_d A\cos\theta & , \pi \le \theta < \theta_2 \\ \mu N & , \theta_2 \le \theta < \theta_3 \\ k_d(B - \delta_1) + k_d A\cos\theta & , \theta_3 \le \theta \le 2\pi \end{cases} \tag{23}$$

Where,

$$\theta_1 = \cos^{-1}\{\frac{k_d(\delta_1 - B) - \mu N}{k_d A}\}$$
$$\theta_2 = 2\pi - \cos^{-1}\{\frac{2\mu N}{k_d A} - 1.\} \quad (24)$$
$$\theta_3 = 2\pi - \cos^{-1}\{\frac{k_d(\delta_1 - B) + \mu N}{k_d A}\}$$

The Fourier coefficients can be derived from equations 23 , 24 as

$$f_b = \frac{1}{2\pi}\{k_d(B - \delta_1)(2\pi + \theta_1 - \theta_3) + \mu N(\theta_1 + \theta_3 - 2\theta_2) + k_d A(\sin\theta_1 + \sin\theta_2 - \sin\theta_3 + \theta_2 - \pi)\}$$

$$f_c = \frac{1}{\pi}\{k_d(B - \delta_1)(\sin\theta_1 - \sin\theta_3) + \frac{k_d A}{2}(\pi + \theta_1 + \theta_2 - \theta_3) + k_d A\sin\theta_2 + \frac{k_d A}{4}(\sin 2\theta_1 + \sin 2\theta_2 - \sin 2\theta_3) + \mu N(\sin\theta_1 + \sin\theta_3 - 2\sin\theta_2)\} \quad (25)$$

$$f_s = \frac{1}{\pi}\{k_d(B - \delta_1)(\cos\theta_3 - \cos\theta_1) + \mu N(2\cos\theta_2 - \cos_3 - \cos\theta_1) + (\frac{k_d A}{4})(\cos 2\theta_3 + 1. - \cos 2\theta_1 - \cos 2\theta_2) - k_d A(1. + \cos\delta_2)\}$$

Case 4. Slip with Lower Limit : $\mu N \le A + B \le \delta_1 + \frac{\mu N}{k_d}$, $A - B \ge \delta_2 + \frac{\mu N}{k_d}$

In this case, the lower stop is hit during the displacement cycle. As before, the nonlinear force f_n can be separated into four sections.

$$f_n = \begin{cases} (\mu N - k_d A) + k_d A\cos\theta & , 0. \le \theta \le \theta_1 \\ -\mu N & , \theta_1 \le \theta \le \theta_2 \\ k_d(B + \delta_2) + k_d A\cos\theta & , \theta_2 \le \theta\ \theta_3 \\ \mu N & , \theta_3 \le \theta \le 2\pi \end{cases} \quad (26)$$

Where

$$\theta_1 = \cos^{-1}\{\frac{k_d A - 2\mu N}{k_d A}\}$$
$$\theta_2 = 2\pi - \cos^{-1}\{-\frac{\mu N + k_d(B+\delta_2)}{k_d A}\} \qquad (27)$$
$$\theta_3 = 2\pi - \cos^{-1}\{\frac{\mu N - k_d(B+\delta_2)}{k_d A}\}$$

From equation 26 and 27, the Fourier coefficients are obtained.

$$f_b = \frac{1}{2\pi}\{\mu N(2\theta_1 - \theta_2 - \theta_3 + 2\pi) + k_d A(\sin\theta_1 + \sin\theta_3 - \sin\theta_2 - \theta_1) + k_d(B+\delta_2)(\theta_3 - \theta_2)\}$$

$$f_c = \frac{1}{\pi}\{\mu N(2\sin\theta_1 - \sin\theta_2 - \sin\theta_3) + k_d(B+\delta_2)(\sin\theta_3 - \sin\theta_2) - k_d A\sin\theta_1 + (\frac{k_d A}{2})(\theta_1 + \theta_3 - \theta_2) + (\frac{k_d A}{4})(\sin 2\theta_1 + \sin 2\theta_3 - \sin 2\theta_2)\} \qquad (28)$$

$$f_s = \frac{1}{\pi}\{\mu N(\cos\theta_2 + \cos\theta_3 - 2\cos\theta_1) + k_d A(\cos\theta_1 - 1.) + k_d(B+\delta_2)(\cos\theta_2 - \cos\theta_3) (\frac{k_d A}{4})(1. + \cos 2\theta_2 - \cos 2\theta_1 - \cos 2\theta_3)\}$$

Case 5. Slip with Both Limit : $A + B \geq \delta_1 + \frac{\mu N}{k_d}$, $A - B \geq \delta_2 + \frac{\mu N}{k_d}$

In this case, both stops are hit during the displacement cycle(Figure 6). As before, the nonlinear force f_n can be divided into five sections.

$$f_n = \begin{cases} k_d(B-\delta_1) + k_d A\cos\theta & , 0. \leq \theta < \theta_1 \\ -\mu N & , \theta_1 \leq \theta < \theta_2 \\ k_d(B+\delta_1) + k_d A\cos\theta & , \theta_2 \leq \theta < \theta_3 \\ \mu N & , \theta_3 \leq \theta < \theta_4 \\ k_d(B-\delta_1) + k_d A\cos\theta & , \theta_4 \leq \theta \leq 2\pi \end{cases} \qquad (29)$$

Where

$$\theta_1 = \cos^{-1}\{\frac{k_d(\delta_1 - B) - \mu N}{k_d A}\}$$
$$\theta_2 = \cos^{-1}\{-\frac{\mu N + k_d(B + \delta_2)}{k_d A}\}$$
$$\theta_3 = 2\pi - \cos^{-1}\{\frac{\mu N - k_d(B + \delta_2)}{k_d A}\} \qquad (30)$$
$$\theta_4 = 2\pi - \cos^{-1}\{\frac{\mu N + k_d(\delta_1 - B)}{k_d A}\}$$

And the Fourier coefficients are derived from 29, 30 as

$$f_b = \frac{1}{2\pi}\{k_d(B - \delta_1)(\theta_1 + 2\pi - \theta_4) + k_d(B + \delta_2)(\theta_3 - \theta_2)$$
$$+ k_d A(\sin\theta_1 + \sin\theta_3 - \sin\theta_2 - \sin\theta_4)$$
$$+ \mu N(\theta_1 + \theta_4 - \theta_2 - \theta_3)\}$$

$$f_c = \frac{1}{\pi}\{k_d(B - \delta_1)(\sin\theta_1 - \sin\theta_4) + (\frac{k_d A}{2})(\theta_1 + \theta_3 + 2\pi - \theta_2 - \theta_4)$$
$$+ (\frac{k_d A}{4})(\sin 2\theta_1 + \sin 2\theta_3 - \sin 2\theta_2 - \sin 2\theta_4)$$
$$+ k_d(B + \delta_2)(\sin\theta_3 - \sin\theta_2)$$
$$+ \mu N(\sin\theta_1 - \sin\theta_2 + \sin\theta_4 - \sin\theta_3)\}$$

$$f_s = \frac{1}{\pi}\{k_d(B - \delta_1)(\cos\theta_4 - \cos\theta_1) + k_d(B + \delta_2)(\cos\theta_2 - \cos\theta_3) \qquad (31)$$
$$+ \mu N(\cos\theta_2 + \cos\theta_3 - \cos\theta_1 - \cos\theta_4)$$
$$+ (\frac{k_d A}{4})(\cos 2\theta_4 + \cos 2\theta_2 - \cos 2\theta_3 \cos 2\theta_1)\}$$

From the above obtained results, the nonlinear force f_n can be written as

$$f_n = f_b(A, B, \mu N, k_d, \delta_1, \delta_2) + f_c(A, B, \mu N, k_d, \delta_1, \delta_2)\cos\theta \qquad (32)$$
$$+ f_s(A, , B, \mu N, k_d, \delta_1, \delta_2)$$

The three coefficients can be nondimensionlized as follows :

$$f_b = \mu N F_b(\alpha, \beta, \gamma, q)$$
$$f_c = \mu N F_c(\alpha, \beta, \gamma, q) \qquad (33)$$
$$f_s = \mu N F_s(\alpha, \beta, \gamma, q)$$

where,

$$\alpha = \frac{k_d A}{\mu N}$$

$$\beta = \frac{B}{\delta}$$

$$\gamma = \frac{k_d \delta}{\mu N} \qquad (34)$$

$$q = \frac{\delta_1}{\delta}$$

where, $\delta = \delta_1 + \delta_2$

References

[1] Griffin, J. H.
Friction Damping of Resonant Stresses in Gas Turbine Engine Airfoils.
Journal of Engineering For Power vol 102(2):329-333, April, 1980.

[2] Iwan, W. D. .
Steady State Dynamic Response of a Limit Slip System.
ASME Journal of Applied Mechanics vol 35:322-326, June, 1968.

[3] Menq,C.-H. , Griffin, J. H. , Bielak, J.
The Influence of a Variable Normal Load on the Forced Vibration of a Frictionally Damped Structure.
ASME Journal of Engineering for Gas Turbines and Power vol 108:300-305, 1986.